Threshold Pion Photoproduction off Nucleons using the Nuclear Model with Explicit Pions

Martin Mikkelsen – 201706771

Master's Thesis

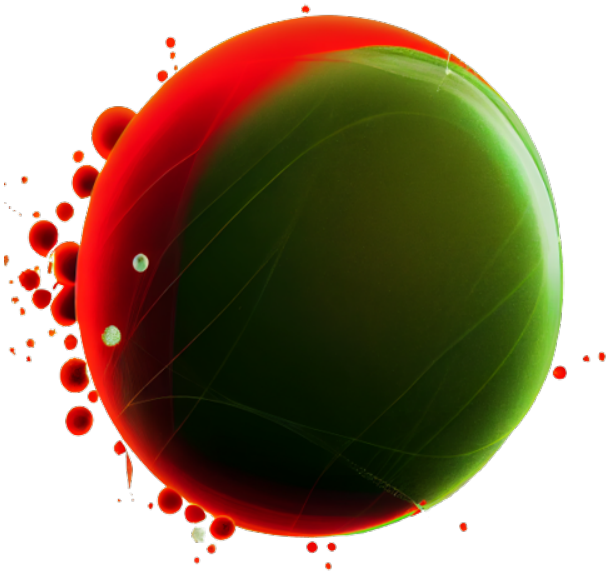

Supervisor: Dmitri Fedorov

Department of Physics and Astronomy
Aarhus University

November 2022

AARHUS
UNIVERSITY
DEPARTMENT OF PHYSICS
AND ASTRONOMY

Colophon

Threshold Pion Photoproduction off Nucleons using the Nuclear Model with Explicit Pions

Master's thesis by Martin Mikkelsen

The project is supervised by Dmitri Fedorov

Typeset by the author using LaTeX and the memoir document class. Figures are made with the using the Seaborn package in Python and the Tikz package.

Code for document, figures and numerical calculations can be found on `https://github.com/MartinMikkelsen`

Printed at Aarhus University

Abstract

This thesis investigates pion photoproduction off nucleons near the threshold using a nuclear model with explicit mesons. In this model, the nucleons do not interact through a potential but emit and absorb mesons which are treated explicitly, and we limit the model to the one meson approximation. We focus on the case where the mesons are pions and calculate the total cross-section of pion photoproduction near the threshold. Specifically, we find the set of parameters for which the model quantitatively can describe the total cross section near the threshold.

We introduce the nuclear model with explicit mesons and describe the advantages of using this model within the regime of few-body, low-energy nuclear physics. We consider a pion-nucleus system where we introduce a phenomenological form factor which depends on a strength parameter and a range parameter. We then consider a numerical approach to solving the Schrödinger equation describing the pion-nucleon system and evaluate how changing the phenomenological form factor will affect the solutions. We also discuss a relativistic expansion of the kinetic operators to deduce the importance of relativistic effects on the pion-nucleon system. We find that the relativistic effects are negligible for most sets of parameters. To further test the model, we introduce a new operator which is inspired by an effective field theory. We find that the operator is compatible with the nuclear model but is also numerically intensive, and perhaps another numerical approach is more suitable for this operator.

We then focus on pion photoproduction and how this can be described within the framework of the nuclear model. As a first approach, we consider a dipole approximation and calculate the total cross-section for the photoproduction of charged pions off protons. We find that the dipole approximation is only valid very close to the threshold. We then consider the central challenge of this thesis: a general expression for the differential cross-section and the total cross-section near the threshold. We compute these expressions for all four pion photoproduction processes. We conclude that the model is able to describe the experimental cross-section for neutral pions off protons quantitatively, and we present the sets of parameters. At the time of writing, no experimental data exists for neutral pion photoproduction off neutrons near the threshold, but a theoretical prediction was made. In the case of charged pion photoproduction off nucleons, expressions for the total cross section and the charge density were found. The model has some problems accurately describing the behaviour of the total cross-section of charged pions, and perhaps the one-pion approximation is insufficient, and further work is needed.

Resumé

Dette speciale undersøger pion-fotoproduktion på nukleoner tæt på tærsklen gennem en kernemodel hvor mesonerne bliver behandlet eksplicit. I denne model vekselvirker nukleonerne ikke gennem et potentiale, men udsender og absorberer mesoner, som er håndteret eksplicit, og vi begrænser modellen til udelukkende at betragte en enkeltmesonapproksimation. Vi fokuserer på det tilfælde, hvor mesonerne er pioner og beregner det totale tværsnit af pion-fotoproduktion tæt på tærsklen. Specifikt bestemmer vi de parametre, for hvilke modellen kvantitativt kan beskrive det totale tværsnit tæt på tærsklen.

Vi introducerer kernemodellen med eksplicitte mesoner og beskriver de fordele denne model har i området af fålegeme, lavenergi kernefysik. Vi betragter et pion-nukleon system, hvor vi introducerer en fænomenologisk formfaktor, som afhænger af en styrkeparameter og en afstandsparameter. Derefter undersøger vi en numerisk fremgangsmåde til at løse Schödingerligningen, som beskriver pion-nukleon systemet og evaluerer hvordan ændringer i formfaktoren vil påvirke løsningerne. Vi diskuterer, også en relativistisk udvidelse af operatoren for kinetisk energi og udleder vigtigheden af relativistiske effekter på pion-nukleon systemet. Vi finder, at relativistiske effekter er ubetydelige for de fleste sæt af parametre. For at teste modellen yderligere introducerer vi en ny operator, som er inspireret af en effektiv feltteori. Modellen er kompatibel med denne operator, men denne er tungere numerisk, og dette indikerer, at en anden numerisk metode kan være bedre egnet til denne operator.

Derefter fokuserer vi på pion-fotoproduktion, og hvordan dette kan blive beskrevet indenfor kernemodellens teoretiske ramme. Som et første mål betragter vi en dipolapproksimation og beregner det totale tværsnit for ladet pion-fotoproduktion fra protoner. Vi kommer frem til at dipolapproksimationen udelukkende gælder meget tæt på tærsklen. Derefter betragter vi hovedudfordringen i dette speciale: et generelt udtryk for differentialtværsnittet og for det totale tværsnit tæt på tærsklen. Vi udleder alle udtrykkene for de fire pion-fotoproduktionsprocesser. Vi konkluderer, at modellen kvantitativt kan beskrive eksperimentelt data for fotoproduktionen af neutrale pioner fra protoner, og vi præsenterer flere sæt af parametre. I skrivende stund er der ikke eksperimentelt data for fotoproduktionen af neutrale pioner fra neutroner tæt på tærsklen, men vi præsenterer en teoretisk model. I tilfældet med ladede pioner finder vi frem til udtryk for det totale tværsnit og ladningstætheden. Undersøgelsen viser også, at modellen har nogle problemer, når det gælder beskrivelsen af tværsnittet af ladede pioner, hvilket indikerer at enkeltpionapproksimationen ikke er tilstrækkelig og der kræves yderligere overvejelser.

Preface

This thesis is the culmination of a year's work at the Department of Physics and Astronomy at Aarhus University under the supervision of Dmitri Fedorov. The objective was to test if the nuclear model with explicit pions could describe pion photoproduction off nucleons near the threshold. I would like to thank my supervisor Dmitri Fedorov for introducing me to the topic and the discussions we had along the way. I have learned a great deal of new theoretical physics combined with numerical implementations.

I would like to thank my friends and office colleagues, Magnus Linnet Madsen, Daniel Holleufer, Anton Lautrup, Ajanthan Ketheeswaran, Freja Nielsen, Lukas M. Wick and Sebastian Yde Madsen for their support and company throughout my time at Aarhus University. A special thanks to Magnus, Daniel and Ajanthan for revising the thesis.

The cover image shows a green nucleon interacting with a red particle, which is the colour distinction we will use throughout. The image was made using an artificial intelligence program that creates images from textual descriptions called Midjourney. The figures in the margin will be used to supplement the text, while the figures in the text generally are the results.

Contents

Chapter 1

Introduction

Nuclear physics covers and expands different ideas from other areas of physics. These include but are not limited to low- and high-energy physics, few- and many-body dynamics, and classical and quantum statistical mechanics. Two concepts are needed when discussing nuclear physics: the nucleon and mesons [1]. Nuclei consist of nucleons and are held together by the nuclear forces – by exchanging mediating quanta called mesons. This is similar to how the photon exchange generates the electromagnetic force. There are many different mesons, but the lightest mesons are called the pions (π^-, π^0, π^+) with a mass of about one-seventh of the nucleon leaving us in the MeV range. This energy scale also defines the regime known as low-energy physics, where the nucleus can be considered non-relativistic, and the mesons are virtual particles hidden in nucleon-nucleon interactions. Generally speaking, within the domain of low-energy nuclear physics, the nucleus appears as a self-bound many-body nucleonic system with intrinsic degrees of freedom. These systems are mesoscopic, along with atoms, molecules, micro- and nano-devices of condensed matter systems, and quantum computers. This means they are sufficiently large to have statistical regularities yet also small enough to study individual quantum states.

Increasing the energy will reveal the intermediate region of nuclear physics. Here relativistic effects become more important, and the meson and nucleon excitations become explicit. This energy scale is loosely characterized by an energy scale of a few GeV. These systems are highly complex and making a useable model describing the system is still a work in progress. This thesis explores a model for describing the low-energy, few-body systems.

1.1 Nuclear Model

In this thesis, we focus on the nuclear model with explicit pions. Previous work acted as a proof-of-concept using sigma mesons and a natural next step of development would be pions due to the lighter mass [2]. The large Compton wavelength of 1.4 fm provides the longest-ranged contribution to the nucleon-nucleon interaction [3]. Furthermore, the pion is a significant component of the nuclear wave function where the pion dominates meson exchange corrections to different nuclear properties.

1.2 Outline of Thesis

This thesis is organized as follows. Chapter 2 will cover the theoretical background needed for the other chapters. This includes how we can describe the interaction of radiation with matter within the framework of the second quantization. This chapter also covers the necessary equations for the density of states where the main results are two expressions, one in the relativistic limit and one in the non-relativistic limit. Chapter 3 will introduce the nuclear model with explicit mesons. We will go through how the nuclear model with explicit mesons will be constructed generally. Next, we consider the case where the mesons are pions and look at how we can determine an equation describing the pion-nucleon system. We then focus specifically on the one-pion approximation, which is the most straightforward appearance of the nuclear model with explicit pions. This is closely related to how we formulate the dressing of the proton and arrive at an equation that is to be solved numerically. This is the subject of section 3.4, where we explore the flexibility of this model. Specifically, this means we test different form factors and do a relativistic expansion to explore how this affects the solutions found in the previous section. Finally, we test how changing the operator to another operator found in effective field theory affects the system. In chapter 4, we explore pion photoproduction using the model with explicit pions and how this emerges naturally as a photodisintegration process. We consider the four possible reactions: two off the proton and two off the neutron. To calculate the matrix elements, we make a dipole approximation in section 4.1, and an exact approach follows in section 4.2. To extract the parameters, we perform fits and compare them to experimental data. Some of the thesis made it into an article [4].

Chapter 2

Theoretical Background

2.1 Interaction of Radiation with Matter

In the following, we will derive the necessary equations describing how a quantised vector field interacts with matter within the framework of the second quantisation. We will assume the final quantised form of the vector potential [1, 5] given by

$$\mathbf{A}(\mathbf{r},t)=\sum_{\mathbf{k},\lambda}\sqrt{\frac{2\pi\hbar c^2}{\omega_{\mathbf{k}}V}}\left(a_{\mathbf{k},\lambda}\,\mathbf{e}_{\mathbf{k},\lambda}\,\mathrm{e}^{i(\mathbf{k}\cdot\mathbf{r})-i\omega_k t}+a^{\dagger}_{\mathbf{k},\boldsymbol{\lambda}}\mathbf{e}^{*}_{\mathbf{k},\lambda}\,\mathrm{e}^{-i(\mathbf{k}\cdot\mathbf{r})+i\omega_k t}\right), \quad (2.1)$$

where $\mathbf{k}$ is a wave vector related to the frequency by the dispersion law $\omega = ck$ and the wave polarisation is described by $\mathbf{e}_{\mathbf{k},\lambda}$. The operators $a_{\mathbf{k},\lambda}$ and $a^{\dagger}_{\mathbf{k},\lambda}$ are the annihilation and creation operators, respectively. The normalisation of these operators yields the factor in front.

We now consider a non-relativistic system of charged particles interacting with the electromagnetic field. In this thesis, we will consider a two-particle system, but in this section, we generalise the results to any number of particles denoted by the subscript i. The interaction will enable the system to emit and absorb photons. We start with the Hamiltonian describing the many-body system given by $H_0(\mathbf{r}_i, \mathbf{p}_i)$ with no field, where $\mathbf{r}_i$ and $\mathbf{p}_i$ is the position and momentum of the i'th particle, respectively. We introduce a field and do the following gauge transform

$$\mathbf{p}_i \rightarrow \mathbf{p}_i - \frac{e_i}{c}\mathbf{A}(\mathbf{r}_i), \quad (2.2)$$

where e_i is the charge of the i'th particle. This leads to a new Hamiltonian, which now depends on the field variables

$$H_0 \rightarrow H_0' = H_0\left(\mathbf{r}_i, \mathbf{p}_i - \frac{e_i}{c}\mathbf{A}(\mathbf{r}_i)\right) + \sum_i e_i\phi(\mathbf{r}_i), \quad (2.3)$$

where the last term in equation (2.3) is the potential energy. We now introduce the radiation gauge choice, which is purely conventional and any other choice of gauge will result in the same equations, albeit more difficult. The radiation gauge [6] is given by

$$\boldsymbol{\nabla}\cdot\mathbf{A} = \phi = 0, \quad (2.4)$$

and the non-relativistic Hamiltonian of the system describing the interaction with the radiation field is given by

$$H = \sum_i \frac{1}{2m_i}\left(\mathbf{p} - \frac{e_i}{c}\mathbf{A}(\mathbf{r}_i)\right)^2, \quad (2.5)$$

where $\mathbf{A}(\mathbf{r}_i)$ is equation (2.1) at point $\mathbf{r}_i$ and m_i is the mass of the i'th particle. We assumed the interaction between particles depends on their coordinates, so the minimal inclusion of the electromagnetic field affects only the kinetic part. This is a fair approximation in the non-relativistic limit and does not account for velocity-dependant interactions such as spin-orbit. The electromagnetic interaction is relatively weak, and its strength is given by the fine structure constant, $\alpha = e^2/(\hbar c)$. Generally speaking, this interaction can be taken into account in the lowest non-vanishing order of perturbation theory. We expand (2.5) and keep only the linear terms

$$H^{(1)} = -\sum_i \frac{e_i}{2m_i c}(\mathbf{p}_i \cdot \mathbf{A}(\mathbf{r}_i) + \mathbf{A}(\mathbf{r}_i) \cdot \mathbf{p}_i), \tag{2.6}$$

where the (1) represents the first non-vanishing order. Due to our choice of gauge equation (2.4) the two terms in (2.6) commute and we are left with

$$H^{(1)} = -\sum_i \frac{e_i}{m_i c}\mathbf{A}(\mathbf{r}_i, t) \cdot \mathbf{p}_i. \tag{2.7}$$

For the type of problems we will be solving in chapter 4, we will be working mainly with a single charged particle, and we can ignore the sum in (2.7).

2.2 Density of States

As mentioned in section 2.1, the electromagnetic interaction strength is related to the fine structure constant. In chapter 4, we want to do perturbation theory to get an expression for the total cross-section as a function of energy which the relatively weak fine structure constant allows. From perturbation theory, the transition rate is described by Fermi's golden rule given by

$$\mathrm{d}\omega = \frac{2\pi}{\hbar}|\mathcal{M}|^2 \rho, \tag{2.8}$$

where the matrix element $\mathcal{M}$ is the subject of chapter 4 and $\mathrm{d}\rho$ is the density of states after the interaction. In this section, we will derive general results of the density of states in the non-relativistic and relativistic limits. The density of states is defined by

$$\rho(E) = \frac{\mathrm{d}n(E)}{\mathrm{d}E}, \tag{2.9}$$

where $n(E)$ is the number of states with energy E. Consider the number of states within the momentum space volume

$$\mathrm{d}^3\mathbf{p} = p^2 \mathrm{d}p\, \mathrm{d}\Omega_q, \tag{2.10}$$

where the subscript q is used to emphasize momentum space. We will use this notation throughout the thesis[1]. Equation (2.10) corresponds to the momenta with magnitude from p to $p + \mathrm{d}p$ and within a cone of solid angle $\mathrm{d}\Omega_q$. This is illustrated in figure 2.1. We use the solutions to the Schrödinger equation for a particle confined in a large volume with periodic boundary conditions are travelling waves [7]. This leads to the following expression

$$\rho(p)\,\mathrm{d}\rho = \left(\frac{L}{2\pi\hbar}\right)^3 \mathrm{d}^3\mathbf{p} = \frac{V}{(2\pi\hbar)^3} p^2\, \mathrm{d}p\, \mathrm{d}\Omega_q. \tag{2.11}$$

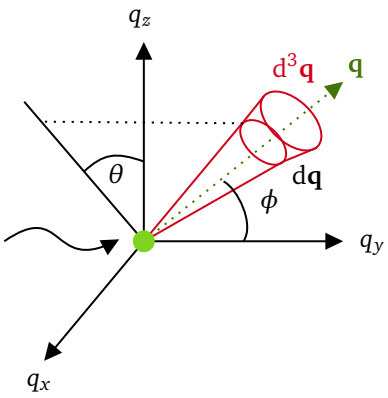

Figure 2.1: Differential cross section and the solid angle Ω_q (red cone).

1. We will write the momentum as $\hbar\mathbf{q}$, where $\mathbf{q}$ is a wave number in chapter 4 so to keep the notation consistent we also use q here.

In chapter 4, we are interested in the number of possible final states with energy in the range between E_f and $E_f + \mathrm{d}E_f$ so we express (2.11) in terms of energy, where the subscript f denotes final state. This is given by [7]

$$\rho(E_f) = \frac{V p_f^2}{(2\pi\hbar)^3} \frac{\mathrm{d}p_f}{\mathrm{d}E_f} \,\mathrm{d}\Omega_q. \tag{2.12}$$

This is the final non-relativistic expression. However, we want to generalise this result to account for relativistic effects. For a general pion photoproduction process, we can write

$$N + \gamma \longrightarrow N + \pi, \tag{2.13}$$

where N is the nucleon and γ is a photon. The final state energy [7] is then given by

$$E_f = E_N + E_\pi = \sqrt{p_f^2 c^2 + m_N^2 c^4} + \sqrt{p_f^2 c^2 + m_\pi^2 c^4}. \tag{2.14}$$

We now change the notation to match the variables used later in chapter 4 and write the final state momentum p_f in terms of the pion-nucleon wave number q. That is, $\mathbf{p} \longrightarrow \hbar\mathbf{q}$.

From conservation of energy, we get the following expression for the energy of the relative pion-nucleon motion denoted E_q in the center of mass.

$$E_q = \sqrt{m_N^2 c^4 + (\hbar c)^2 q^2} + \sqrt{m_\pi c^4 + (\hbar c)^2 q^2} - m_N c^2 - m_\pi c^2. \tag{2.15}$$

Examining (2.12), we want an expression for the final state momentum in terms of the wave number. The density of states around $\mathbf{q}$ is given by

$$\rho_f = \frac{Vq}{(2\pi)^3} \frac{1}{2} \frac{\mathrm{d}q^2}{\mathrm{d}E_q} \mathrm{d}\Omega_q. \tag{2.16}$$

We now solve for $(\hbar c)^2 q^2$ in (2.15), which yields the following result[2]

$$(\hbar c)^2 q^2 = \frac{E_q(E_q + 2m_N c^2)(E_q + 2m\pi c^2)(E_q + 2m_N c^2 + 2m_\pi c^2)}{4(E_q + m_N c^2 + m_\pi c^2)^2}, \tag{2.17}$$

and we are now able to calculate the derivative of equation (2.17)

$$\begin{aligned}(\hbar c)^2 \frac{\mathrm{d}q^2}{\mathrm{d}E_q} = {} & \frac{(E_q^2 + 2E_q m_N c^2 + 2m_N^2 c^4 + 2E_q m_\pi c^2 + 2m_N m_\pi c^4)}{2(E_q + m_N c^2 + m_\pi c^2)^3} \\ & \times (E_q^2 + 2E_q m_N c^2 + 2m_\pi^2 c^4 + 2E_q m_\pi c^2 + 2m_N m_\pi c^4),\end{aligned} \tag{2.18}$$

which yields the final expression for the relativistic density of states by substituting equation (2.18) into equation (2.16). Non-relativistically, the density of states in terms of E_q and q is given by the following

$$\mathrm{d}\rho_f = \frac{Vq\mu_{N\pi}}{(2\pi)^3\hbar^2} \mathrm{d}\,\Omega_q, \tag{2.19}$$

where $\mu_{N\pi}$ is the reduced mass of the pion-nucleon system. We now have two expressions for the density of states to use in conjunction with equation (2.8). In chapter 4, we will refer to equation (2.18) as the relativistic density of states and equation (2.19) as the non-relativistic density of states.

2. It is also possible to use the approximation that $\sqrt{x^2 + y^2} \simeq 0.96x + 0.4y$ yielding an error of only 4%.

Chapter 3

The Nuclear Model with Explicit Mesons

We consider a nuclear model where the nucleus is held together by emitting and absorbing mesons, and the mesons are treated explicitly [2]. We are considering the regime of low-energy nuclear physics, and this model is different from conventional interaction models in several ways. Firstly, the nucleons interact by emitting and absorbing mesons, not via a phenomenological potential. Conceptually this is similar to the one-boson-exchange model. Secondly, the number of parameters is greatly reduced. Regardless of the meson type, the number of parameters is two; the range and the strength of the meson-nucleon coupling are denoted b and S, respectively. In the case of the pion, the central force, tensor force and the three-body force are all concealed within these two parameters. This model should be able to reproduce phenomena within the realm of low-energy nuclear physics, such as the deuteron, nucleon-nucleon scattering, pion-nucleon scattering and pion photoproduction. The low energy regime also enables the use of the Schrödinger equation to describe the equations of motion. The model must be constructed in a way such that usual quantum numbers are conserved; this means conservation of isospin, angular momentum and parity.

3.1 Nuclear Interacting Model with Explicit Pions

In the following, we focus on the nuclear model with explicit pions [2]. The pion is the lightest of the strongly interacting particles with a mass of about 15% of the nucleon mass. This yields a large Compton wavelength of 1.4 fm, which provides the longest-ranged contribution to the nucleon-nucleon interaction [3]. Furthermore, the pion is a significant component of the nuclear wave function where the pion dominates meson exchange corrections to different nuclear properties. In general, the bare nucleon is surrounded by several virtual pions.

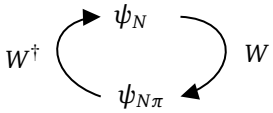

Figure 3.1: Illustration of the pion-nucleon operators, W, $W^\dagger$.

They are virtual in the same sense that the positron-electron pair are virtual in pair creation from a photon. It is important to stress that these are virtual since they can have properties impossible for real particles. The multi-component wave function of the nucleon can be written as

$$\Psi_N = \begin{bmatrix} \psi_N \\ \psi_{N\pi} \\ \psi_{N\pi\pi} \\ \vdots \end{bmatrix}, \tag{3.1}$$

where ψ_N is the bare nucleon, and the other wave functions are dressed by an arbitrary number of pions indicated by the subscripts. Assuming the nuclear interaction conserves isospin, angular momentum and parity, we can construct the following operator for the pion-nucleon operator [8]

$$W \equiv (\boldsymbol{\tau} \cdot \boldsymbol{\pi})(\boldsymbol{\sigma} \cdot \mathbf{r}) f(r) \tag{3.2}$$

$$W^\dagger \equiv \int_V \mathrm{d}^3 r \, (\boldsymbol{\tau} \cdot \boldsymbol{\pi})^\dagger (\boldsymbol{\sigma} \cdot \mathbf{r})^\dagger f(r), \tag{3.3}$$

where $\boldsymbol{\tau}$ is the isovector of Pauli matrices acting on the nucleon in isospin space and $\boldsymbol{\sigma}$ is the same but for spin space and $\mathbf{r}$ is the relative coordinate distance between the nucleon and the pion. Note that the $W^\dagger$ operator contains an integral to remove the coordinate of the annihilated pion. These operators ensure the conservation of isospin, angular momentum and parity. The isovector of pions is denoted $\boldsymbol{\pi}$ and can be combined with $\boldsymbol{\tau}$ and be represented as a 2-by-2 hermitian matrix [9] given by

$$\boldsymbol{\tau} \cdot \boldsymbol{\pi} = \tau_0 \pi_0 + \sqrt{2}\tau_- \pi^+ \sqrt{2}\tau_+ \pi^- = \begin{bmatrix} \pi^0 & \sqrt{2}\pi^- \\ \sqrt{2}\pi^+ & -\pi^0 \end{bmatrix}, \tag{3.4}$$

where the isospin coefficients will be important later when we discuss different photoproduction processes. Similarly, by expanding the matrices in spin space and using the spherical tensor operator, we get the following matrix in terms of the spherical harmonics

$$\boldsymbol{\sigma} \cdot \mathbf{r} = \sqrt{\frac{4\pi}{3}} r \begin{bmatrix} Y_1^0 & \sqrt{2}Y_1^{-1} \\ \sqrt{2}Y_1^1 & Y_1^0 \end{bmatrix}, \tag{3.5}$$

where similar to the isospin space, the off-diagonals include a factor $\sqrt{2}$.

There is also a phenomenological, short-range form factor $f(r)$ [8] given by

$$f(r) = \frac{S}{b} \mathrm{e}^{-r^2/b^2}, \tag{3.6}$$

where S and b are the pion-nucleon coupling strength and range, respectively. These are illustrated in figure 3.2. The action of annihilating a pion must include the integral over coordinate space to remove the coordinate. We now have everything we need to construct a general Hamiltonian for the multi-component wave function of the nucleon in (3.1)

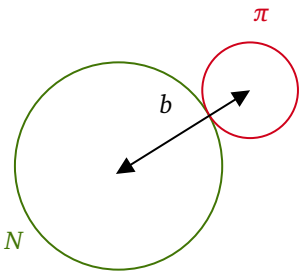

Figure 3.2: Schematic figure of the pion-nucleon system with a range parameter b.

$$H = \begin{bmatrix} K_N & W^\dagger & 0 & \dots \\ W & K_N + K_\pi + m_\pi c^2 + V_C & W^\dagger & \dots \\ 0 & W & K_N + K_{\pi(1)} + K_{\pi(2)} + 2m_\pi c^2 + V_C & \dots \\ \vdots & \vdots & \vdots & \ddots \end{bmatrix}, \tag{3.7}$$

where the kinetic operators are given by

$$K_N = \frac{-\hbar^2}{2m_N c^2} \frac{\partial^2}{\partial \mathbf{R}^2} \tag{3.8}$$

$$K_\pi = \frac{-\hbar^2}{2m_\pi c^2} \frac{\partial^2}{\partial \mathbf{r}^2}. \tag{3.9}$$

Note the different derivatives–here $\mathbf{R}$ is the centre-of-mass coordinate, and $\mathbf{r}$ is the relative coordinate. The subscripts on the kinetic operators in (3.7) represent the order in which the pions are created. If charged

particles are involved, one must include a Coulomb interaction denoted by V_C. From (3.1) and (3.7) we can construct the general Schrödinger equation

$$H\Psi_N = E\Psi_N, \tag{3.10}$$

where the ground state is the bare nucleon surrounded by virtual pions. The ground state energy in the rest frame of the nucleon gives the mass of the physical nucleon. Within the framework of this model, one can generate a physical pion by supplying enough energy such that the pion is no longer virtual. The pion is trapped behind a potential barrier of height $m_\pi c^2 = 140$ MeV and cannot leave unless this or more energy is supplied to the system. This is illustrated in figure 3.3.

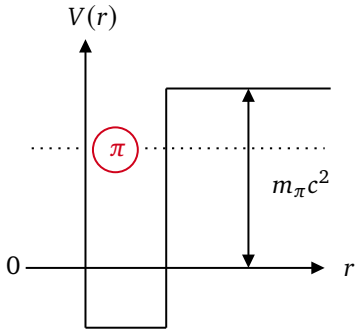

Figure 3.3: Illustration of the virtual pion.

3.2 Dressing of the Nucleon in the One Pion Approximation

We now consider the scenario where a photon interacts with the nucleon-pion systems and generates a physical pion. This means the energy supplied by the photon is higher than the potential barrier also when recoil effects are taken into account. This also hints towards how a pion photoproduction process would emerge naturally as a disintegration process in this nuclear model. To generate more pions, the photon energy would have to be increased by the same amount. This also means that the first pion is responsible for the most significant contribution to the nucleon dressing. This will be referred to as the one-pion approximation. As a proof-of-concept, we constrain ourselves to the one pion approximation and adding more pions should, in principle, be a straightforward extension of the following derivations.

Returning to (3.1) and enforcing the one-pion approximation yields

$$\Psi = \begin{bmatrix} \psi_N(\mathbf{R}) \\ \psi_{N\pi}(\mathbf{r}) \end{bmatrix}. \tag{3.11}$$

The Hamiltonian, which acts on the two-component wave function in (3.11) is given by[1]

$$H = \begin{bmatrix} K_N & W^\dagger \\ W & K_N + K_\pi + m_\pi c^2 \end{bmatrix}, \tag{3.12}$$

So far, we have kept the model as simple as possible by expressing the equations in terms of the nucleon. From now on, we treat the nucleon as two states of the same strongly interacting object with an intrinsic degree of freedom which defines the proton and neutron. We choose the proton and neutron as

$$|p\rangle = \begin{bmatrix} 1 \\ 0 \end{bmatrix} \quad |n\rangle = \begin{bmatrix} 0 \\ 1 \end{bmatrix}. \tag{3.13}$$

Furthermore, we denote the spin state of the nucleon by an arrow

$$|\uparrow\rangle = \begin{bmatrix} 1 \\ 0 \end{bmatrix} \quad |\downarrow\rangle = \begin{bmatrix} 0 \\ 1 \end{bmatrix}. \tag{3.14}$$

The wave function must also be normalised to one nucleon per unit volume. This is as far as we get in general terms for the dressing of the nucleon in the one-pion approximation.

1. Strictly speaking, one should use a three-component wave function to account for the mass difference between π^0 and $\pi^\pm$. This is done in appendix A. This shows that the effects of accounting for the mass difference between the pions are negligible.

3.3 Dressing of the Proton

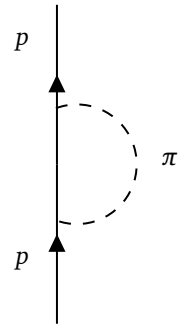

Figure 3.4: Feynman diagram of the dressing of the proton.

We now focus our attention on the dressing of the proton in the spin-up state shown as a Feynman diagram in figure 3.4. The calculations are almost identical, remembering the definitions from section 3.2. The wave function of the bare proton can thus be written as

$$\psi_p = \frac{p\uparrow}{\sqrt{V}}, \tag{3.15}$$

where we omit the kets to unclutter the notation. The Hamiltonian (3.12) suggest the following expression for the wave function of the pion-nucleon system

$$\psi_{N\pi} = (\boldsymbol{\tau}\cdot\boldsymbol{\pi})(\boldsymbol{\sigma}\cdot\mathbf{r})\frac{p\uparrow}{\sqrt{V}}\phi(r), \tag{3.16}$$

where $\phi(r)$ is the spatial wave function which will play an integral part in the rest of this section. From (3.2), we can construct the Schrödinger equation of the system

$$\begin{bmatrix} K_p & W^\dagger \\ W & K_N + K_\pi + m_\pi c^2 \end{bmatrix}\begin{bmatrix} \psi_p \\ \psi_{N\pi} \end{bmatrix} = E\begin{bmatrix} \psi_p \\ \psi_{N\pi} \end{bmatrix}. \tag{3.17}$$

Note that the kinetic operator in the second row still contains K_N to emphasise that this acts on the general nucleon-pion wave function, $\psi_{N\pi}$. Expanding (3.17) yields two equations

$$K_p\psi_p + W^\dagger\psi_{N\pi} = E\psi_p \tag{3.18}$$

$$W\psi_p + (K_N + K_\pi + m_\pi c^2)\psi_{N\pi} = E\psi_{N\pi}. \tag{3.19}$$

In the rest frame of the proton, the center-of-mass dependency vanishes and inserting the operator (3.2) yields

$$\int_V \mathrm{d}^3r\,(\boldsymbol{\tau}\cdot\boldsymbol{\pi})^\dagger(\boldsymbol{\sigma}\cdot\mathbf{r})^\dagger f(r)\phi(r)(\boldsymbol{\tau}\cdot\boldsymbol{\pi})(\boldsymbol{\sigma}\cdot\mathbf{r})p\frac{1}{\sqrt{V}} = Ep\frac{1}{\sqrt{V}}, \tag{3.20}$$

where the integration comes from equation (3.3). This can be further simplified using relations for the matrix vectors[2]

2. $(\boldsymbol{\tau}\cdot\boldsymbol{\pi})^\dagger(\boldsymbol{\tau}\cdot\boldsymbol{\pi}) = 3$ and $(\boldsymbol{\sigma}\cdot\mathbf{r})^\dagger(\boldsymbol{\sigma}\cdot\mathbf{r}) = r^2$

$$12\pi\int_0^\infty \mathrm{d}r\, f(r)\phi(r)r^4 = E. \tag{3.21}$$

Similarly for (3.19) where the term $K_N\psi_{N\pi}$ vanishes,

$$\begin{aligned}(\boldsymbol{\tau}\cdot\boldsymbol{\pi})(\boldsymbol{\sigma}\cdot\mathbf{r})f(r)p\frac{1}{\sqrt{V}} - \frac{\hbar^2}{2\mu_{N\pi}}\nabla^2_{\mathbf{r}}(\boldsymbol{\tau}\cdot\boldsymbol{\pi})(\boldsymbol{\sigma}\cdot\mathbf{r})p\frac{1}{\sqrt{V}}\phi(r) \\ = (E - m_\pi c^2)(\boldsymbol{\tau}\cdot\boldsymbol{\pi})(\boldsymbol{\sigma}\cdot\mathbf{r})\phi(r)p\frac{1}{\sqrt{V}},\end{aligned} \tag{3.22}$$

using (3.9) and where $\mu_{N\pi}$ is the reduced mass of the nucleon-pion system. This equation can be further simplified by using a vector operator relation which yields[3]

3. $\nabla^2(\mathbf{r}\phi(r)) = \mathbf{r}\left(\frac{\mathrm{d}^2\phi(r)}{\mathrm{d}r^2} + \frac{4}{r}\frac{\mathrm{d}\phi(r)}{\mathrm{d}r}\right)$

$$f(r) - \frac{\hbar^2}{2\mu_{N\pi}}\left(\frac{\mathrm{d}^2\phi(r)}{\mathrm{d}r^2} + \frac{4}{r}\frac{\mathrm{d}\phi(r)}{\mathrm{d}r}\right) = (E - m_\pi c^2)\phi(r). \tag{3.23}$$

This means equation (3.21) and (3.23) are the two equations that must be solved numerically.

$$\left.\begin{aligned} &12\pi\textstyle\int_0^\infty \mathrm{d}r\, f(r)\phi(r)r^4 = E \\ &f(r) - \frac{\hbar^2}{2\mu_{N\pi}}\left(\frac{\mathrm{d}^2\phi(r)}{\mathrm{d}r^2} + \frac{4}{r}\frac{\mathrm{d}\phi(r)}{\mathrm{d}r}\right) + m_\pi c^2\phi(r) = E\phi(r)\end{aligned}\right\} \tag{3.24}$$

The bracket on the right is used to emphasize that (3.24) is a coupled system.

3.4 Numerical Considerations

To solve the system of equations (3.24), one can consider two different numerical approaches. One approach presents a more intuitive picture of how to solve this equation, while the other is more robust and practical.

For a given E, one can solve the second-order differential equation corresponding to $\phi(E)$. Conversely, for a given $\phi(r)$, one can compute the integral to find $E(\phi)$. This leads to the fixed-point equation given by

$$E(\phi(E)) = E, \tag{3.25}$$

which is a single variable non-linear equation. Equation (3.25) can be solved using a root-finding algorithm. This approach is generally not as efficient since the algorithm will have to search through a large parameter space to obtain a suitable solution.

The second approach consists of reformulating the system in equation (3.24) as a boundary value problem with the following conditions

$$I'(r) = 12\pi f(r)\phi(r)r^4, \quad I(0) = 0,\ I(\infty) = E, \tag{3.26}$$

where I is the integral in equation (3.24). Essentially, the boundary conditions we require for the energy are written in equation (3.26). The equation starts from a singular point and extends to infinity. We require the solution to stay finite, which means approximations are needed at both limits. At $r \to 0$, the differential equation is approximately an Euler-Cauchy equation with basis solutions 1 and r^{-1}. For finite solutions, the latter is ignored, which means $\phi'(a) = 0$ is the requirement for $a \approx 0$.[4] For $r \to \infty$, the dominating term in the differential equation is

$$-\phi''(r) + 2\mu_{N\pi}(m_\pi c^2 - E)\phi(r) = 0. \tag{3.27}$$

Since we expect a negative value for E, the basis solutions are on the form

$$\phi(r) = \exp\left\{\pm\sqrt{2\mu_{N\pi}(m_\pi c^2 + |E|)}\right\}r. \tag{3.28}$$

In the case of a positive sign, the solution diverges. For the basis solution with negative exponents, we have

$$\phi'(r) + \sqrt{2\mu_{N\pi}(m_\pi c^2 + |E|)}\phi(r) = 0. \tag{3.29}$$

These two conditions are suitable boundary conditions for the left and right boundaries, respectively. The algorithm [10, 11] converges, and a solution to (3.17) is found. The solutions can be seen in figure 3.5 for the parameters $S = 10$ MeV and $b = 1$ fm.

4. You would end up with the same conclusion if you consider $\phi = a + r^n$ and plug this into $\phi'' + 4\phi'/r = 0$, which yields $n = 0, -1$.

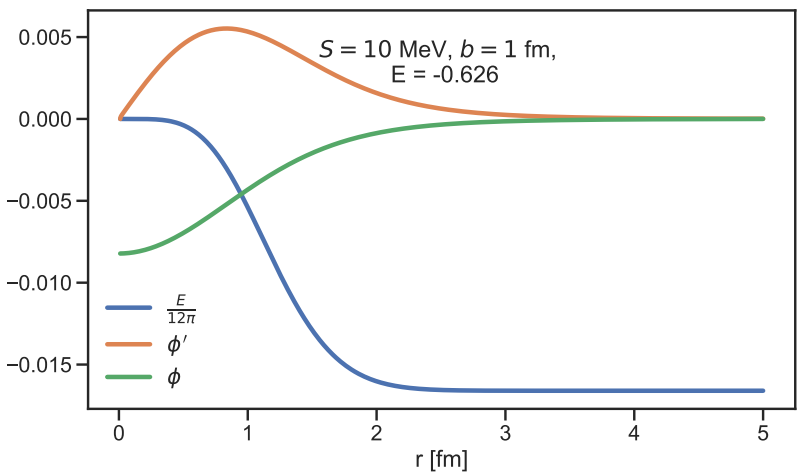

Figure 3.5: Boundary value problem solutions. The energy (blue line) is scaled.

Also, note that since we expect the energy to be less than zero, it makes sense for the wave function to be negative since all other terms in the integral in equation (3.24) are positive. It might appear strange to have a negative wave function, $\phi(r)$, but there are two things to note. One can add an arbitrary phase to equation (3.11) and flip the sign. Also, for all computations, we are only interested in the norm-square of the wave function. The energy for the parameters shown in figure 3.5 is $E = -0.626\,\text{MeV}$ and this value is very sensitive to the parameters S and b since they enter in the form factor as seen in equation (3.6). Furthermore, as mentioned in section 3.1, this gives the physical mass of the proton–its importance will be clear later when comparing the mass contribution from virtual pion in chapter 4.

Since we cannot allow the wave function to extend to infinity numerically, we must introduce some cut-off. Since the wave function of the pion-nucleon system has a built-in range parameter b, it is natural to let the cut-off be proportional to this parameter. Within the regime of nuclear physics, we expect the wave function to extend up to a length within the order of magnitude of 10 fermi. Quantitatively this means a small constant of proportionality in front of r_{min} and another constant in front of r_{max}. Numerically, a constant of proportionality for r_{max} and the impact can be seen in figure 3.6 where the radial wave functions stop after $5r_{\text{max}}$.

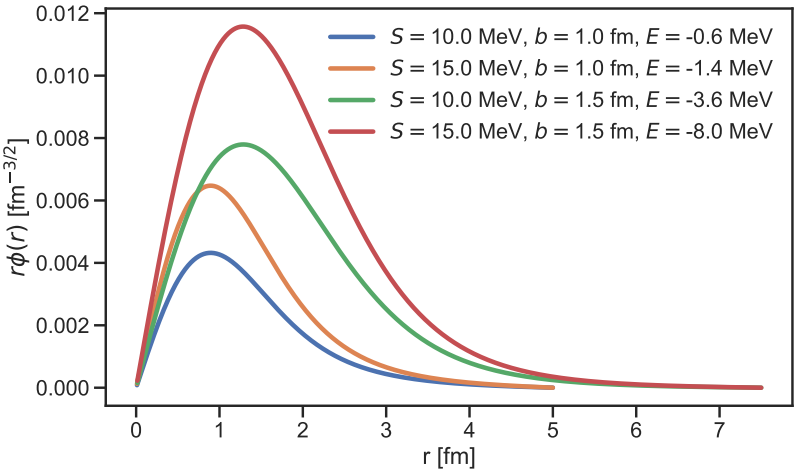

Figure 3.6: Radial wave function for different parameters S and b to illustrate the behavoir on the radial function.

Figure 3.6 also illustrates the behaviour of the radial wave functions as the parameters change. As the coupling strength parameter S increases, the radial wave function increases. As the range parameter b increases, the peak is shifted to this new value. We can figure out the units of the radial wave function since the following integral must be dimensionless

$$\int_V \mathrm{d}^3R \int_V \mathrm{d}^3r \left|\psi_{N\pi}\right|^2, \tag{3.30}$$

which means the wave function $\phi(r)$ must have dimensions of $\text{fm}^{-5/2}$, and the radial wave function $r\phi(r)$ must have dimensions of $\text{fm}^{-3/2}$. Note that the two integrals come from the annihilation of a pion and the normalisation of one particle per unit volume, respectively.

3.4.1 Different Form Factors

Compared to conventional interaction models of the nucleus, this model has the advantage of having very few parameters. The phenomenological form factor $f(r)$ only consists of an interaction strength S and a range parameter b. The form factor can take many forms, yielding different wave function solutions and changing the energy. The formalism in section 3.4 is very flexible to changes in the form factor, and here we explore how different form factors impact the wave function. The form factors must all decrease as a function of r since we constrain the system to short-range forces. The solutions in figure 3.6 assume the form factor from equation (3.6), which is Gaussian. A priori, we do now know anything about the form factor, and it might as well be Yukawa-like.

$$f(r) = \frac{S}{b}\frac{\exp\left\{-\frac{r}{b}\right\}}{r}. \tag{3.31}$$

Figure 3.7 shows the radial wave functions if the form factor is Yukawa like

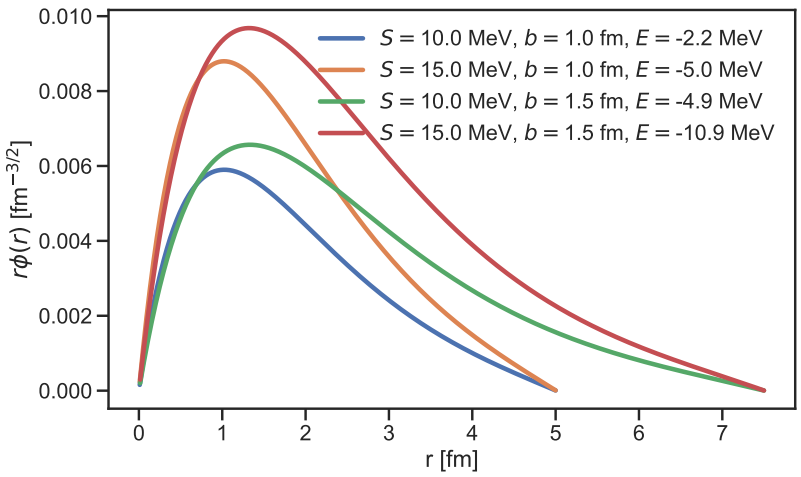

Figure 3.7: Radial wave functions for different parameters as shown in the legend.

The shapes of the radial wave functions are similar to the Gaussian case, but the energies do not match due to the r^2/b^2 dependency in the Gaussian case. One could argue for a Yukawa-like form factor but with a gaussian exponential, $\exp\left(r^2/b^2\right)/r$. The energies are the same within a few MeV, but this defeats the purpose of a Yukawa form. An exponential form factor would make the radial wave function too long to describe the nuclear range since we are constrained to about 15 fm.

3.4.2 Relativistic Expansion

As described in section 3.1, we are using the Schrödinger equation, which hints at a non-relativistic limit of the pion-nucleon system. We also know the pion is virtual, which means under a potential barrier. An avant-garde idea is to do a relativistic expansion of the kinetic term, which depends on the relative coordinate **r**.

The pion is virtual, which makes the velocity of the particle hard to estimate. Nonetheless, we can do an expansion of the kinetic operator and see how this affects the model. To account for relativistic effects, we

can replace the kinetic term, $K_{\mathbf{r}}$ in (3.17)

$$K_{\mathbf{r}} \to K_{\mathbf{r},\text{rel}} = \sqrt{p^2c^2 + \mu_{N\pi}^2 c^4} = \mu_{N\pi}c^2\left(\sqrt{1 + \frac{p^2}{\mu_{N\pi}^2 c^2}} - 1\right), \tag{3.32}$$

where $\mu_{N\pi}$ is the reduced mass of the nucleon-pion system. This leads to a new system of equations, and these solutions can be compared to the non-relativistic limit to deduce which relativistic regime dominates the system. Starting from (3.19)

$$f(r)(\boldsymbol{\tau}\cdot\boldsymbol{\pi})(\boldsymbol{\sigma}\cdot\mathbf{r})\psi_p + \mu_{N\pi}c^2\left(\sqrt{1 + \frac{p^2}{\mu_{N\pi}^2 c^2}} - 1\right)\psi_{N\pi} = (E - m_\pi c^2)\psi_{N\pi}, \tag{3.33}$$

This equation turns out to be divergent, and we must therefore resort to an approximation. The kinetic energy is expanded

$$K_{\mathbf{r},\text{rel}} = \mu_{N\pi}c^2\sqrt{1 + \frac{p^2}{\mu_{N\pi}^2}} - \mu_{N\pi}c^2 \approx \frac{p^2}{2\mu_{N\pi}} - \frac{p^4}{8\mu_{N\pi}^3 c^2} \tag{3.34}$$

This means we get an extra term in (3.22), yielding

$$\begin{aligned}(\boldsymbol{\tau}\cdot\boldsymbol{\pi})(\boldsymbol{\sigma}\cdot\mathbf{r})f(r)\frac{p\uparrow}{\sqrt{V}} + \left(\frac{p^2}{2\mu_{N\pi}} - \frac{p^4}{8\mu_{N\pi}^3 c^2}\right)(\boldsymbol{\tau}\cdot\boldsymbol{\pi})(\boldsymbol{\sigma}\cdot\mathbf{r})\frac{p\uparrow}{\sqrt{V}}\phi(r) \\ = (E - m_\pi c^2)(\boldsymbol{\tau}\cdot\boldsymbol{\pi})(\boldsymbol{\sigma}\cdot\mathbf{r})\phi(r)\frac{p\uparrow}{\sqrt{V}},\end{aligned} \tag{3.35}$$

5. $\nabla^4(\mathbf{r}\phi(r)) = \mathbf{r}\left(\phi^{(4)} + \frac{6}{r}\phi^{(3)}\right)$

Using the vector operators yields the following expression[5]

$$\begin{aligned}f(r) - \frac{\hbar^2}{2\mu_{N\pi}}\left(\phi^{(2)}(r) + \frac{4}{r}\phi^{(1)}(r)\right) - \frac{\hbar^4}{8\mu_{N\pi}^3 c^3}\left(\phi^{(4)}(r) + \frac{6}{r}\phi^{(3)}(r)\right) \\ = (E - m_\pi c^2)\phi(r),\end{aligned} \tag{3.36}$$

where the exponent, (n), is the order of the differentiation. This leads to a system of equations given by

$$\left.\begin{aligned}&12\pi\int_0^\infty \mathrm{d}r\, f(r)\phi(r)r^4 = E \\ &f(r) - \tfrac{\hbar^2}{2\mu_{N\pi}}\left(\phi^{(2)}(r) + \tfrac{4}{r}\phi^{(1)}(r)\right) - \tfrac{\hbar^4}{8\mu_{N\pi}^3 c^3}\left(\phi^{(4)}(r) + \tfrac{6}{r}\phi^{(3)}(r)\right) = (E - m_\pi c^2)\phi(r)\end{aligned}\right\} \tag{3.37}$$

This system is a fourth-order differential equation coupled to an integrodifferential equation and is solved using the boundary value problem technique. The boundary conditions can be found using the same considerations as in the previous section. For $r \to \infty$ the dominating terms are

$$\phi^{(4)}(r) = \frac{-8\mu_{N\pi}c^2}{\hbar^4}(E - m_\pi c^2)\phi(r) - \frac{4\mu_{N\pi}^2 c^2}{\hbar^2}\phi(r)^{(2)} \tag{3.38}$$

The solutions are shown in figure 3.8.

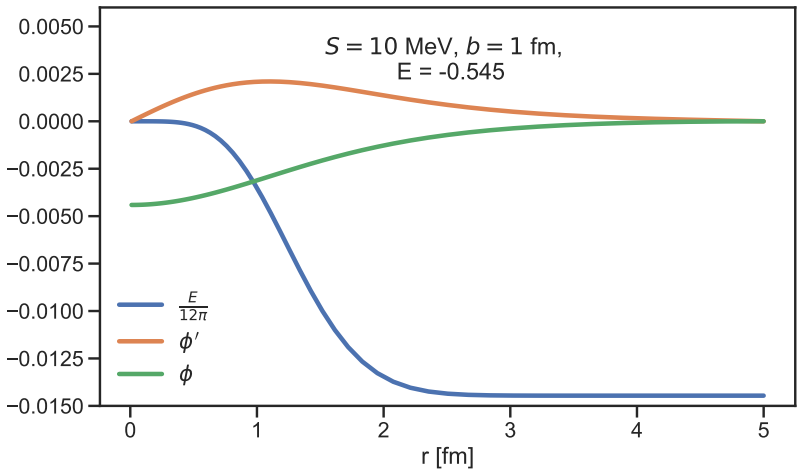

Figure 3.8: Boundary value problem solutions for the relativistic expansion using the Gaussian form factor. The energy convergence is scaled.

We gain information about the system both from the wave function and the energy, and we consider these two components of figure 3.8 separately. The radial wave function of the system can be seen in figure 3.9

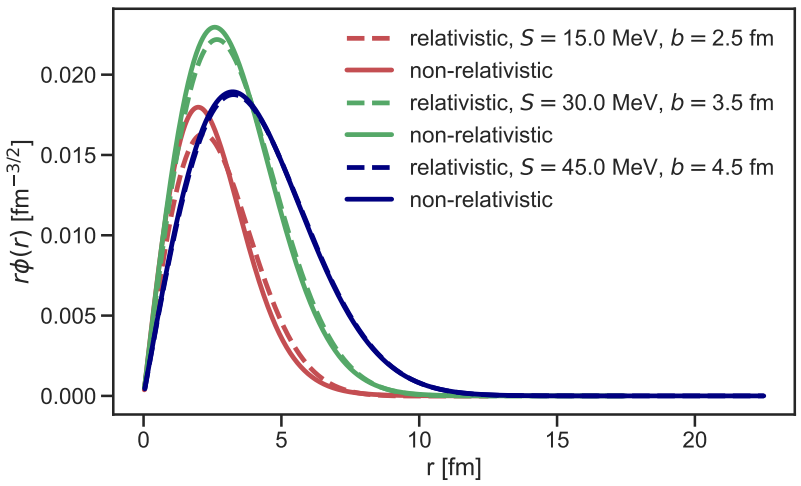

Figure 3.9: Relativistic (dashed) and non-relativistic radial wave functions for three different parameters. The matching colours have the same parameters.

The radial wave functions are similar, with the lowest strength parameter S and range parameter b having the largest difference. This can be explained by considering equation (3.37). The form factor $f(r)$ depends explicitly on the ratio between these two parameters in the same way in the relativistic limit as in the non-relativistic limit. However, the form factor can change by orders of magnitude by varying the two parameters, which will only affect the solution $\phi(r)$ when the form factor vanishes and the $r \to \infty$ limit applies. This also means we should expect the energy ratio between the non-relativistic equation (3.24) and equation (3.37) to approach 1 as the range parameter b increases since this decreases the impact of the form factor. This is shown in figure 3.10, where the energy ratio is given by

$$E_R = \frac{E_{\text{relativistic}}}{E_{\text{non-relativistic}}}. \tag{3.39}$$

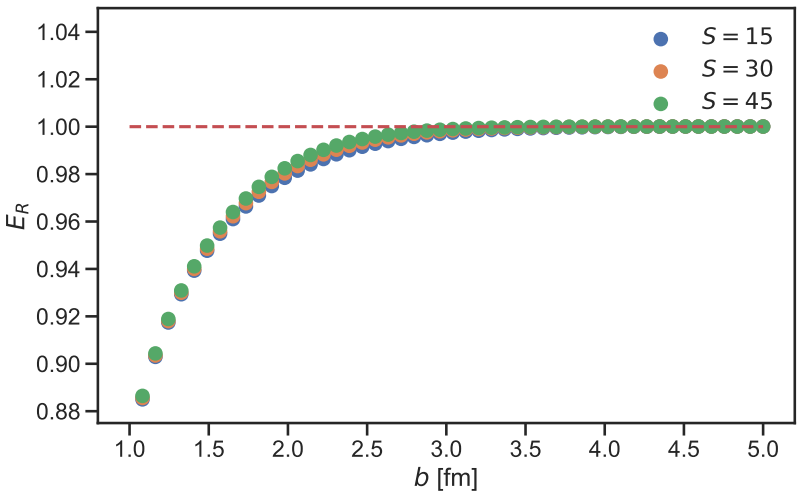

Figure 3.10: The energy ratio $E_{\text{rel}}/E_{\text{nonrel}}$ shown as a function of the range parameter b for a Gaussian form factor given by equation (3.6)

We can apply the same logic to the system of equations with a Yukawa-like form factor as in equation (3.31), and we expect the same convergence. This is shown on figure 3.11.

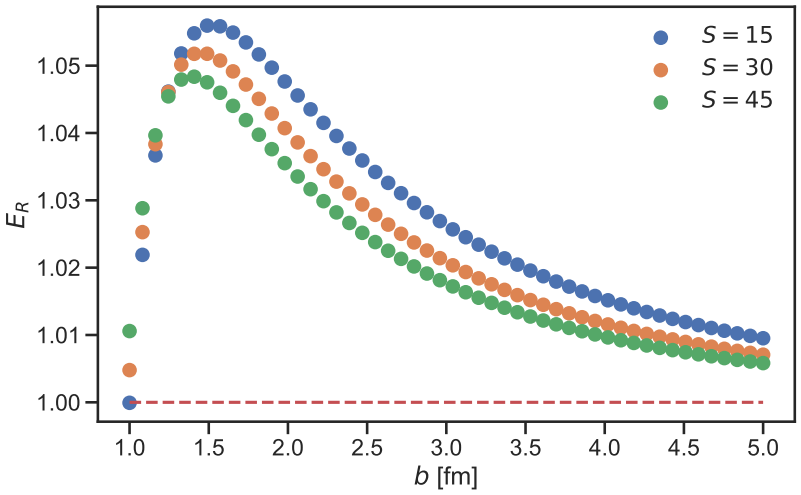

Figure 3.11: The energy ratio $E_{\text{rel}}/E_{\text{nonrel}}$ shown as a function of the range parameter b for a Yukawa-like form factor given by equation (3.31).

The pion is virtual and hence in a classically forbidden region, but we can still estimate which relativistic regime dominates the system. Both in terms of the radial wave function and in terms of the energy ratio, relativistic effects are negligible. This result holds for different form factors since they must all decrease as a function of r.

Considering figure 3.10, we see the maximum discrepancy between the relativistic and the non-relativistic energy is about 10 per cent and decreases rapidly. This means relativistic effects vanish as we increase the range parameter b. A physical explanation of this could be that as we increase the spatial dimension, a virtual pion with the same kinetic energy would have a lower velocity and hence behave less relativistically. This analysis is supported if the same behaviour is not present when we keep b fixed and increase S. This is shown in figure 3.12 for the Gaussian form factor.

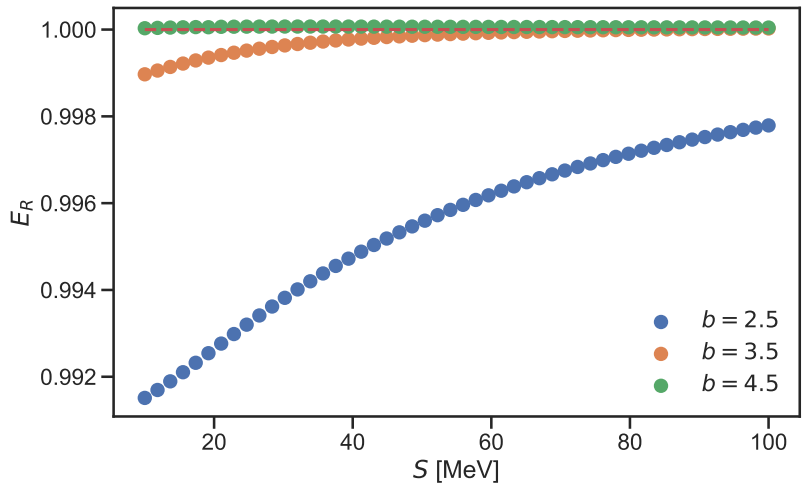

Figure 3.12: The energy ratio $E_{\text{rel}}/E_{\text{nonrel}}$ shown as a function of the strength parameter b for a Gaussian form factor given by equation (3.6).

We can produce a similar plot for the Yukawa-like form factor is shown in figure 3.13

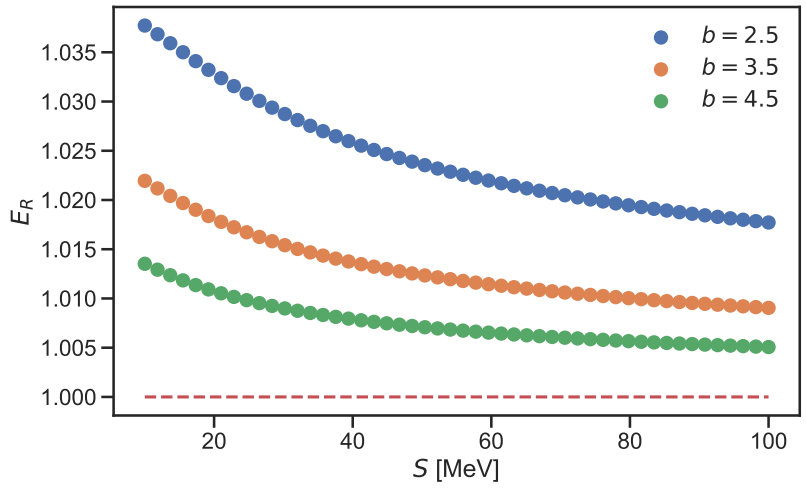

Figure 3.13: The energy ratio $E_{\text{rel}}/E_{\text{nonrel}}$ shown as a function of the strength parameter S for a Yukawa-like form factor given by equation (3.31).

We have now tested what happens if we do a relativistic expansion of the kinetic operators and make changes to the form factor. From section 3.1, we know that the nuclear interaction must conserve isospin, angular momentum and parity, but this can be achieved in numerous ways. In the following section, we will create a new operator inspired by a chiral effective field theory.

3.4.3 Nuclear Effective Field Theory Operator

The construction of the most general chiral Lagrangian is based on the theory of the non-linear realisation of symmetry [12]. We will not attempt to derive this result but refer to [12, 13, 14, 15]

The baryon-number-conserving chiral Lagrangian can be split into pieces with even numbers of fermion fields. In this section, we will focus on

$$\mathcal{L} = N^\dagger \left(i\mathcal{D}_0 + \frac{\mathcal{D}^2}{2m_N} \right) N + \frac{g_A}{2f_\pi} N^\dagger (\boldsymbol{\tau} \cdot \boldsymbol{\sigma})(\mathbf{D} \cdot \boldsymbol{\pi}) N, \tag{3.40}$$

where $N = (p\ n)^{\mathrm{T}}$, $\mathcal{D}$ and D are the covariant derivatives for the nucleon and pion, respectively, m_N is the mass of the nucleon, g_A is the interaction

strength, and f_π is the pion decay constant. The rest of the terms are similar to the creation operator W from equation (3.2)–only the $\mathbf{r}$ is replaced by $\nabla_\mathbf{r}$ in the low-energy regime. The general operator is constructed in such a way that parity, isospin and spin are conserved. In this section, we explore the differences by constructing the nuclear model with explicit mesons with the operator as defined in chiral effective field theory. We assume the following form of the wave function of the proton and the system consisting of a nucleon and a single pion

$$\psi_p = p \uparrow \frac{1}{\sqrt{V}}, \quad \psi_{N\pi} = (\boldsymbol{\tau}\cdot\boldsymbol{\pi})(\boldsymbol{\sigma}\cdot\frac{\partial}{\partial\mathbf{r}})p \uparrow \frac{1}{\sqrt{V}}\phi(r), \tag{3.41}$$

which can be compared to equation (3.15) and equation (3.16). We now construct an operator to create and annihilate a pion

$$W = (\boldsymbol{\tau}\cdot\boldsymbol{\pi})(\boldsymbol{\sigma}\cdot\frac{\partial}{\partial\mathbf{r}})f(r) \tag{3.42}$$

$$W^\dagger = \int_V \mathrm{d}^3r\,(\boldsymbol{\tau}\cdot\boldsymbol{\pi})^\dagger(\boldsymbol{\sigma}\cdot\frac{\partial}{\partial\mathbf{r}})^\dagger f(r), \tag{3.43}$$

where $f(r)$ is a form factor. The annihilation operator must contain the integral to remove the coordinate of the pion. This leads to the following Schrödinger equation

$$\begin{bmatrix} K_\mathbf{R} & W^\dagger \\ W & K_\mathbf{R} + K_\mathbf{r} + m_\pi c^2 \end{bmatrix}\begin{bmatrix}\psi_p \\ \psi_{N\pi}\end{bmatrix} = E\begin{bmatrix}\psi_p \\ \psi_{N\pi}\end{bmatrix}, \tag{3.44}$$

which, when expanded, yields

$$12\pi\int_0^\infty \mathrm{d}r\,\frac{\partial^2}{\partial r^2}r^2 f(r)\phi(r) = E \tag{3.45}$$

$$\frac{\partial}{\partial r}f(r) - \frac{2\hbar^2}{\mu_{N\pi}}\frac{\partial^3}{\partial r^3}\phi(r) = (E - m_\pi c^2)\frac{\partial}{\partial r}\phi(r). \tag{3.46}$$

Assuming the form factor is on the following form

$$f(r) = \frac{S}{b}\mathrm{e}^{-r^2/b^2}, \tag{3.47}$$

will yield the following derivatives

$$\frac{\partial}{\partial r}f(r) = \frac{-2r}{b^2}f(r), \quad \frac{\partial^2}{\partial r^2}f(r) = -\frac{2(b^2 - 2r^22)}{b^4}f(r). \tag{3.48}$$

Thus the terms inside the integral in equation (3.45) are

$$\begin{aligned}\frac{\partial^2}{\partial r^2}(r^2 f(r)\phi(r)) &= 2rf(r)\phi(r) + 2rf'(r)\phi(r) + r^2 f(r)\phi'(r) \\ &\quad + 2rf'(r)\phi(r) + r^2 f''(r)\phi(r) + r^2 f'(r)\phi'(r) \\ &\quad + 2rf(r)\phi(r) + r^2 f'(r)\phi'(r) + r^2 f(r)\phi''(r) \\ &\quad \equiv Y(r).\end{aligned} \tag{3.49}$$

Considering the limits of (3.46) which for large r is

$$\phi'''(r) = \frac{-\mu_{N\pi}}{2\hbar^2}(E - m_\pi c^2)\phi'(r). \tag{3.50}$$

The radial wave function solution is shown on figure 3.14 for different parameters.

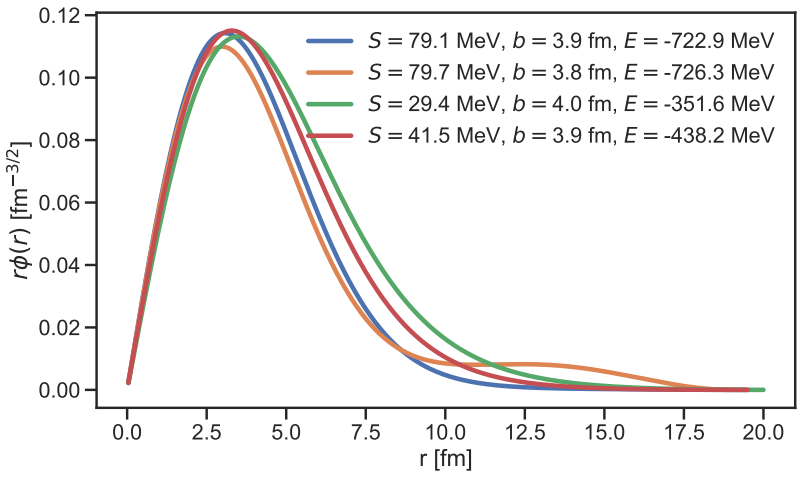

Figure 3.14: The radial wave function using the operator form from an effective field theory.

The parameters S and b in the radial wave functions are not the same as in figure 3.6 and figure 3.7 but should better represent actual parameter values when performing the fit to the total cross-section data. This is done better to highlight this model's validity and some disadvantages. The energies are within the same order of magnitude as when using the model described in section 3.3. There is a difference in energy, and this model could be investigated further – however, using the nuclear effective field theory's operator is a lot more numerically intensive. Due to the derivative in equation (3.41), (3.42) and (3.43), we got many more terms as seen in (3.49), which all have to be integrated numerically. Perhaps another numerical method is better suited for this operator type.

Chapter 4

Pion Photoproduction

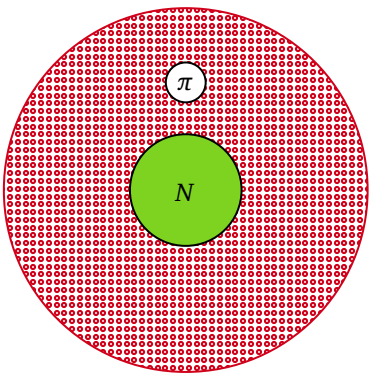

Figure 4.1: Illustration of the dressed nucleon. In the centre (green) is a nucleon, and surrounding it is a cloud of virtual pions (red field).

We now consider the case of pion photoproduction. In the model mentioned in section 3.1 the nucleon is in a superposition of states with an arbitrary number of pions. However, we constrain the model to the one-pion approximation. This is illustrated in figure 4.1

There are four pion photoproduction processes on nucleons, and these are given by

$$p\gamma \rightarrow p\pi^0 \tag{4.1}$$
$$p\gamma \rightarrow n\pi^+ \tag{4.2}$$
$$n\gamma \rightarrow n\pi^0 \tag{4.3}$$
$$n\gamma \rightarrow p\pi^-. \tag{4.4}$$

Within the framework of this model, we would anticipate these processes by applying equation (3.4) to the isospin state of the given nucleon, i.e.

$$(\boldsymbol{\tau}\cdot\boldsymbol{\pi})p = p\pi^0 + \sqrt{2}n\pi^+, \tag{4.5}$$

for the isospin state of the proton and similarly for the neutron. As mentioned in section 3.3, the pion is trapped behind a potential barrier of height 140 MeV and cannot leave unless an incoming photon of sufficient energy hits the pion-nucleon system and photodisintegrates the virtual pion and creates a physical pion in the process. This means pion photoproduction comes naturally as a photodisintegration process. Consider some initial bound state represented by the following two-component wave function

$$|\Phi_i\rangle = \begin{bmatrix} \phi_p \\ \phi_{N\pi} \end{bmatrix}, \tag{4.6}$$

where ϕ represents a bound state. The final state consists of the same superposition but in an unbound system represented by ψ, i.e.

$$|\Psi_f\rangle = \begin{bmatrix} \psi_p \\ \psi_{N\pi} \end{bmatrix}. \tag{4.7}$$

The two-component wave function photodisintegration is similar to the photodisintegration process of the deuteron[1]. We can apply a similar approach and get an expression for the total cross section as a function of photon energy and the strength parameter S, and the range parameter b. The general idea is to fit the parameters to experimental data such that we get a set of parameters within which the model can describe the total cross-section near the threshold. We constrain the model to only apply near the threshold since we expect more pions are needed to describe the total cross-section at higher energies adequately. The

1. This is covered in appendix B.

advantages of this model are twofold: the reduced number of parameters allows us to fit the model to experimental data efficiently, and the model's generality will enable us to apply these parameters to a different process accounting only for the difference in mass and isospin coefficient. In the case of the pion photoproduction process (4.1) is very well investigated [16, 17, 18, 19, 20] while (4.2) and (4.3) have limited data [20] and (4.4) has none near the threshold. Our first approach is to apply a dipole approximation since we are considering the photoproduction processes near the threshold.

4.1 Dipole Approximation

We want to compute the total cross-section of pion photoproduction off nucleons. In this section, we focus on the process involving charged pions off protons given by equation (4.2). The general idea is to use Fermi's golden rule (2.8), and this involves a matrix element

$$\left\langle \Psi_f \middle| \mathbf{d} \middle| \Phi_i \right\rangle, \tag{4.8}$$

where $\mathbf{d}$ is the dipole operator. Equation (4.8) means we use the dipole operator on some initial bound state, and the final state consists of an unbound system. We start from the general expression of the multi-component wave function and impose a normalisation to both the initial and final state. Starting from (4.6)

$$\Phi = \mathcal{N}\begin{bmatrix} p\uparrow \\ (\boldsymbol{\tau}\cdot\boldsymbol{\pi})(\boldsymbol{\sigma}\cdot\mathbf{r})p\uparrow \phi(r) \end{bmatrix}, \tag{4.9}$$

where $\uparrow$ represents the spin state, $\phi(r)$ is the wave function and $\mathcal{N}$ is the normalisation constant. In the pion-nucleon channel, the system is a superposition of $(p\pi^0)$ and $(n\pi^+)$ as dictated by isospin conservation (4.5). The following normalisation is done by requiring the following

$$\begin{aligned} \langle\Phi|\Phi\rangle &= |\mathcal{N}|^2 \left(\left\langle \phi_p \middle| \phi_p \right\rangle + \left\langle \phi_{N\pi} \middle| \phi_{N\pi} \right\rangle \right) && (4.10)\\ &= |\mathcal{N}|^2 \left(V + 3V \int \mathrm{d}^3 r\, r^2 \phi(r)^2 \right) && (4.11)\\ &\stackrel{!}{=} 1. && (4.12) \end{aligned}$$

This leads to the following normalisation constant

$$\mathcal{N} = \frac{1}{\sqrt{V}} \frac{1}{\sqrt{1+\epsilon}}, \tag{4.13}$$

where V is the volume and ϵ is the integral in (4.11)–numerically, this is close to unity. This expression is the properly normalised initial state.

The final state consists of the unbound system represented by ψ. We know the final state consists of a plane wave with wave number $\mathbf{q}$ propagating along the z-axis. The wave number $\mathbf{q}$ is written in terms of the pion-nucleon momentum, and the magnitude of this is given by

$$\frac{\hbar^2 q^2}{2\mu_{N\pi}} = \hbar\omega - m_\pi c^2, \tag{4.14}$$

which is also illustrated in figure 4.2. Equation (4.14) also represents the fact that the energy of the photon must be larger than the mass of the pion to disintegrate the pion-nucleon system. Using the wave number q, the plane wave can be written as

$$\mathrm{e}^{iqz} = \mathrm{e}^{i\mathbf{q}\cdot\mathbf{r}}, \tag{4.15}$$

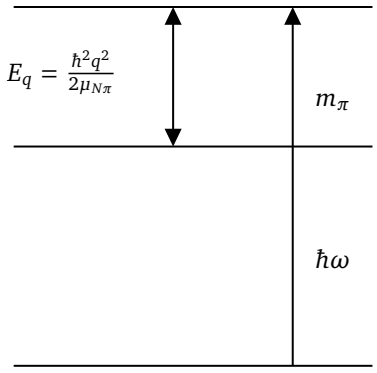

Figure 4.2: Energy diagram of the system. Here $\mu_{N\pi}$ is the reduced mass of the pion-nucleon system.

where θ is the angle between $\mathbf{q}$ and $\mathbf{r}$. Using orthogonality and the addition theorem for the spherical harmonics, we can decompose the plane wave into a Bessel function and spherical harmonics[2]. This yields

2. See equation (C.9)

$$\frac{1}{\sqrt{V}}e^{-i\mathbf{q}\cdot\mathbf{r}} = \frac{1}{\sqrt{V}}\sum_{\ell,m} 4\pi i^{\ell} Y_{\ell}^{*m}(\mathbf{q}) Y_{\ell}^{m}(\mathbf{r}) j_{\ell}(qr) \tag{4.16}$$

$$= \frac{1}{\sqrt{V}}\sum_{\ell} 4\pi i^{\ell} j_{\ell}(qr)\left(\frac{2\ell+1}{4\pi}\right) P_{\ell}(\cos\theta), \tag{4.17}$$

where P_ℓ is the Legendre polynomial of degree ℓ. Since we are considering the energies close to the threshold, we expect mainly the S-wave to contribute and ignore higher orders[3]. We should emphasise that this is an approximation, and a priori, we do not know to what degree this holds. In terms of the expansion (4.16), this greatly simplified the expression

3. Threshold behaviour when $\lambda \simeq 1/q \gg R$ where R is the range. Higher orders of ℓ are generally not important [21].

$$\frac{1}{\sqrt{V}}e^{i\mathbf{q}\cdot\mathbf{r}} \overset{\ell=0}{=} \frac{1}{\sqrt{V}} j_0(qr). \tag{4.18}$$

As equation (4.18) shows, we are left with a spherical Bessel function in the final state where the volume is kept to stress that the total cross section must be independent of the volume. To compute the matrix element, we return to equation (2.1) and consider the electric field given by

$$\boldsymbol{\mathcal{E}} = -\frac{1}{c}\frac{\partial \mathbf{A}}{\partial t}. \tag{4.19}$$

The interaction operator in the dipole approximation is given by

$$H_{\text{dipole}} = -\boldsymbol{\mathcal{E}}(\mathbf{r}=0)\cdot\mathbf{d}, \tag{4.20}$$

where $\mathbf{d}$ is the dipole moment of the pion-nucleon system given by

$$\mathbf{d} = e\frac{\mu_{N\pi}}{m_\pi}\mathbf{r}. \tag{4.21}$$

The general setup for the system is shown in figure 4.3, where the nucleon, in this case, is a proton. Considering a general pion photoproduction process on the form

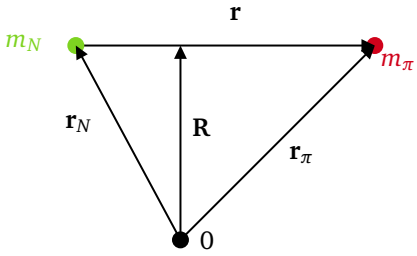

Figure 4.3: Relative coordinates of the pion-nucleon system.

$$N + \gamma \longrightarrow N + \pi \tag{4.22}$$

allows us to compute the electromagnetic part of the matrix element. The initial state consists of the dressed nucleon, and a photon $a^{\dagger}_{\mathbf{k},\lambda}|0\rangle$, where $|0\rangle$ is the electromagnetic vacuum state, $\mathbf{k}$ is the wave number and λ the polarisation index. The final state consists of a nucleon, a pion and the electromagnetic vacuum. This means the transition in the dipole approximation is given by

$$\langle 0|\boldsymbol{\mathcal{E}} a^{\dagger}_{\mathbf{k},\lambda}|0\rangle = \sqrt{\frac{2\pi\hbar}{\omega_k V}} i\omega_k \mathbf{e}_{\mathbf{k},\lambda} e^{-i\omega_k t}, \tag{4.23}$$

which combined with Fermi's golden rule

$$d\omega = \frac{2\pi}{\hbar}|\mathcal{M}|^2 \rho, \tag{4.24}$$

describes the probability per unit of time of making a transition. Equation (4.23) is the most general expression we can make, and in this section,

consider the S-wave channel for the process (4.2). Computations for (4.1), (4.3) and (4.4) are very similar. Computing the matrix element

$$\mathcal{M} = \langle \frac{j_0(qr)}{\sqrt{V}} n\pi^+(\uparrow\downarrow)|H_{\text{dipole}}|\psi_{N\pi}\mathcal{N}\rangle \tag{4.25}$$

Plugging in equation (4.25) and (4.9)

$$\mathcal{M} = -i\omega_k\sqrt{\frac{2\pi\hbar}{V\omega_{\mathbf{k}}}}\mathbf{e}_{\mathbf{k},\lambda}\,\langle \frac{1}{\sqrt{V}} j_0(qr) n\pi^+(\uparrow\downarrow)|\mathbf{d}|(\boldsymbol{\tau}\cdot\boldsymbol{\pi})(\boldsymbol{\sigma}\cdot\mathbf{r})p\uparrow\phi(r)\mathcal{N}\rangle \tag{4.26}$$

where the two arrows represent the two spin states of the neutron and the proton. The different spin states of the neutron in the final state yield two contributions to the total matrix element given by

$$\mathcal{M}^{\uparrow} = \frac{-i\mathcal{N}\sqrt{2}\omega_k\mathbf{e}_{\mathbf{k},\lambda}}{V}\sqrt{\frac{2\pi\hbar}{V\omega_{\mathbf{k}}}}\sqrt{\frac{4\pi}{3}}\,\langle j_0(qr)|d_0 r Y_1^0|\phi(r)\rangle \tag{4.27}$$

$$\mathcal{M}^{\downarrow} = \frac{-i\mathcal{N}2\omega_k\mathbf{e}_{\mathbf{k},\lambda}}{V}\sqrt{\frac{2\pi\hbar}{V\omega_{\mathbf{k}}}}\sqrt{\frac{4\pi}{3}}\,\langle j_0(qr)|d_0 r Y_1^1|\phi(r)\rangle\,, \tag{4.28}$$

where the spin-down state picks up a factor $\sqrt{2}$ from equation (3.5). Now we compute the remaining matrix elements,

$$\begin{aligned}\left\langle j_0(qr)\middle|d_0 r_0\middle|\phi(r)\right\rangle &= \frac{\mu_{N\pi}}{m_\pi} e\left\langle j_0(qr)\middle|r_0 r_0\middle|\phi(r)\right\rangle && (4.29)\\ &= \frac{\mu_{N\pi}}{m_\pi} e\frac{4\pi}{3}\left\langle j_0\middle|r^2\middle|\phi(r)\right\rangle && (4.30)\\ &= \frac{4\pi\mu_{N\pi}e}{3m_\pi}\underbrace{\int_0^\infty \mathrm{d}r\, j_0(qr) r^4\phi(r)}_{Q(r)}, && (4.31)\end{aligned}$$

where the dipole operator (4.21) has been inserted and the angular integrals evaluated. We have also introduced an integral, which contains the wave function $\phi(r)$. Similarly, for the next matrix element,

$$\begin{aligned}\left\langle j_0(qr)\middle|d_- r_+\middle|\phi(r)\right\rangle &= \frac{\mu}{m_\pi} e\left\langle j_0(qr)\middle|r_- r_+\middle|\phi(r)\right\rangle && (4.32)\\ &= \frac{4\pi\mu e}{3m_\pi}\left\langle j_0(qr)\middle|r^2 Y_1^{-1} Y_1^1\middle|\phi(r)\right\rangle && (4.33)\\ &= \frac{4\pi\mu e}{3m_\pi} Q(r). && (4.34)\end{aligned}$$

It turns out that these two matrix elements are equal. Taking the norm-square of (4.31)

$$\left|\mathcal{M}^{\uparrow}\right|^2 = \left(\frac{4\pi\mu e}{3m_\pi}\right)^2 \frac{2\mathcal{N}^2\omega_k(2\pi\hbar)}{V^2}(\mathbf{e}_{\mathbf{k},\lambda})^0(\mathbf{e}^*_{\mathbf{k},\lambda})^0 Q(r)^2 \tag{4.35}$$

Similarly, for the equation (4.34)

$$\left|\mathcal{M}^{\downarrow}\right|^2 = \left(\frac{4\pi\mu e}{3m_\pi}\right)^2 \frac{4\mathcal{N}\omega_{\mathbf{k}}(2\pi\hbar)}{V^2}(\mathbf{e}_{\mathbf{k},\lambda})^+(\mathbf{e}^*_{\mathbf{k},\lambda})^+ Q(r)^2. \tag{4.36}$$

Computing the total matrix element using a polarization theorem[4]

$$\begin{aligned}|\mathcal{M}|^2 &= \left|\mathcal{M}^{\uparrow}\right|^2 + \left|\mathcal{M}^{\downarrow}\right|^2 && (4.37)\\ &= \frac{2\pi\hbar\omega_k\mathcal{N}^2e^2}{V^2}\left(\frac{4\pi\mu}{3m_\pi}\right)^2 Q(r)^2, && (4.38)\end{aligned}$$

4. $(\mathbf{e}^*_{\mathbf{k},\lambda}\cdot\mathbf{e}_{\mathbf{k},\lambda}) = \delta_{\lambda,\lambda'}$ and $\mathbf{e}_{\mathbf{k},\mp} = \pm\frac{1}{\sqrt{2}}(\mathbf{e}_{\mathbf{k},1} \pm i\mathbf{e}_{\mathbf{k},2})$. This leads to $(\mathbf{e}^{0*}_{\mathbf{k},\lambda}\cdot\mathbf{e}^0_{\mathbf{k},\lambda'}) + (\mathbf{e}^{0+}_{\mathbf{k},\lambda}\cdot\mathbf{e}^+_{\mathbf{k},\lambda'}) = \delta_{\lambda,\lambda'} + \frac{1}{2}\delta_{\lambda,\lambda'}$

which is the final expression for the matrix element. According to Fermi's golden rule (4.24) and the non-relativistic density of states (2.19), we get the transition probability. To go from the transition probability to the differential cross-section, we need to consider the flux density of the photons. This means a factor of V/c. This leads to the final expressions for the differential cross-section.

$$\frac{\mathrm{d}\sigma^+}{\mathrm{d}\Omega_q} = \frac{16\pi}{9}\mathcal{N}^2\alpha\frac{kq\mu_{N\pi}^3}{m_\pi^2\hbar c}Q(r)^2, \tag{4.39}$$

where the + is used to indicate that this is the expression for positively charged pions in the final state. Since there is no explicit angular dependency, the total cross-section is given by

$$\sigma^+_{\text{dipole}} = \oint_{4\pi}\frac{\mathrm{d}\sigma}{\mathrm{d}\Omega_q}\mathrm{d}\Omega_q \tag{4.40}$$

$$= \frac{64\pi^2}{9}\mathcal{N}^2\alpha\frac{kq\mu_{N\pi}^3}{m_\pi^2\hbar c}\left(\int_0^\infty \mathrm{d}r\, j_0(qr)r^4\phi(r)\right)^2. \tag{4.41}$$

This is the final expression for the total cross-section of the photoproduction of charged pions using the dipole approximation. We now perform a fit to experimental data for the parameters S and b that enter in the wave function $\phi(r)$. Here two considerations are needed. Both the dipole approximation and the one-pion approximation limit the validity of the cross-section to near the threshold. Quantitatively the dipole approximation holds when

$$\lambda \simeq 1/q \gg R, \tag{4.42}$$

where R is the range of the system. In nuclei, the condition (4.42) is equivalent to

$$\hbar\omega \ll 165A^{1/3}, \tag{4.43}$$

where A is the nucleon number. This limits our dipole approximation's area of validity to approximately 15 MeV from the threshold. Equation (4.41) is fitted to experimental data for the parameters S and b using [10, 22]. The results are shown in figure 4.4. Data is from [20].

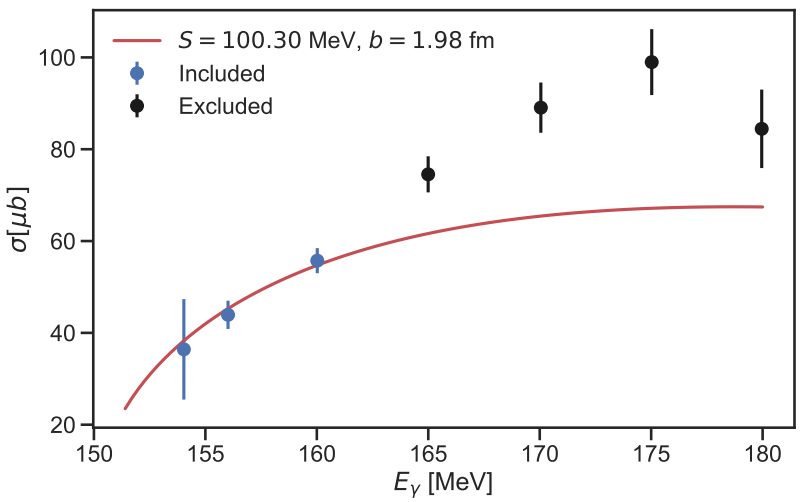

Figure 4.4: The total cross-section of the photoproduction process $\gamma p \to \pi^+ n$ fitted to experimental data. The fit parameters are shown in the figure. The blue data points are included in the fit, and the black data points are excluded since these violate both the dipole and the one-pion approximation. Data is from [20]

Note here that we have used two approximations that limit (4.41) to energies very close to the threshold. We need a more general expression for the cross-section and more data points to test the model's validity further. This means we have to consider the exact matrix element for

the transition and consider the photoproduction of neutral pions off protons since this is the most experimentally investigated photoproduction process.

4.2 Exact Matrix Element

In section 4.1, we investigated how to use the model described in section 3.1 to get an expression for the cross-section, which was compared to experimental data. More specifically, we used the dipole approximation, which introduces a trade-off between the difficulty of the computations and the regime in which our solution is valid. We expect the dipole approximation to hold for energies just above the threshold. To both validate and generalise this result, we now take a different approach and compute the exact cross-section and also consider recoil effects and apply this approach to the four photoproduction processes using the density of states in the non-relativistic and relativistic limits. Strictly speaking, recoil effects should also be considered in section 4.1 since the mass ratio between the nucleon and the pion cannot be assumed to yield a stationary nucleon after the pion photoproduction process.

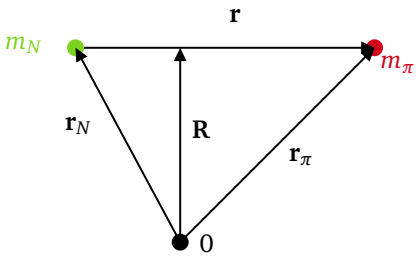

Figure 4.5: Sketch of the system. Here $\mathbf{r}_N$ is the coordinate of the proton and $\mathbf{r}_\pi$ is the coordinate of the pion. The relative coordinate is given by $\mathbf{r} = \mathbf{r}_\pi - \mathbf{r}_N$ and the coordinate of the center-of-mass is $\mathbf{R} = (m_N\mathbf{r}_N + m_\pi\mathbf{r}_\pi)/(m_N + m_\pi)$. The total mass is denoted $M_{N\pi} = m_N + m_\pi$.

To compute the exact matrix elements, we consider a non-relativistic system of particles interacting with the electromagnetic field as described in section 2.1. We have to remember that equation (2.7) describes how a particle with charge interacts with the electromagnetic field. If we consider a process where the initial state is a dressed neutron, the pion must be responsible for the interaction with the electromagnetic field. We will consider the four pion photoproduction processes separately even though the computations are very similar. In general, we will consider a system illustrated in figure 4.5, which shows the pion-nucleon system, and in terms of the Jacobi coordinates, we get the following expressions for the coordinates of the particles

$$\mathbf{r}_N = \mathbf{R} - \frac{m_\pi}{M_{N\pi}}\mathbf{r} \tag{4.44}$$

$$\mathbf{r}_\pi = \mathbf{R} + \frac{m_N}{M_{N\pi}}\mathbf{r}, \tag{4.45}$$

where $\mathbf{R}$ is the coordinate of the center of mass of the pion-nucleon system given by

$$\mathbf{R} = \frac{m_N\mathbf{r}_N + m_\pi\mathbf{r}_\pi}{M_{N\pi}}, \quad M_{N\pi} = m_N + m_\pi. \tag{4.46}$$

The relative coordinate is given by

$$\mathbf{r} = \mathbf{r}_\pi - \mathbf{r}_N. \tag{4.47}$$

The general approach is the same as in section 3.3, where we want to use Fermi's golden rule to compute the total cross-section. In this section, we also consider the impact of changing the density of states to the relativistic case. Furthermore, we estimate the relative weight of the pion component in the wave function of the dressed nucleon. We do this by introducing the following

$$C(\psi_{N\pi}) = \int_V \mathrm{d}^3R \int_V \mathrm{d}^3r \left|\psi_{N\pi}\right|^2, \tag{4.48}$$

where per construction of the model, this is dimensionless. We also introduce a parameter to estimate the virtual pions' contribution to the mass of the dressed nucleon. This will be denoted Π and corresponds to the energy found by solving (3.24).

4.2.1 Neutral Pion Photoproduction off Protons

We are considering the process

$$p\gamma \to \pi^0 p, \tag{4.49}$$

where the proton interacts with the electromagnetic field. The Feynman diagram is shown in figure 4.6. From equation (2.7) we get

$$H^{(1)} = -\frac{e}{m_p c}\mathbf{A}(\mathbf{r}_p, t)\cdot\mathbf{p}_p, \tag{4.50}$$

To calculate the exact matrix el where $\mathbf{p}_p$ is the momentum operator of the proton. Equation (4.50) can be rewritten in terms of the relative coordinates

$$H^{(1)} = -\frac{e}{m_p c}\mathbf{A}\left(\mathbf{R} - \frac{m_\pi}{M_{p\pi}}\mathbf{r}, \mathbf{t}\right)\cdot\left(\frac{m_p}{M_{p\pi}}\mathbf{P} - \mathbf{p}\right) \tag{4.51}$$

In equation (4.49), the initial state consists of a dressed proton and a plane wave photon in the state $a^\dagger_{\mathbf{k},\lambda}|0\rangle$. The final state consists of a proton and a π^0 in a relative plane wave motion. The electromagnetic part of the matrix element is

$$-\frac{e}{m_p c}\langle 0|\mathbf{A}(\mathbf{r}_p, t)a^\dagger_{\mathbf{k},\lambda}|0\rangle = -\frac{e}{m_p c}\sqrt{\frac{2\pi\hbar}{\omega_k V}}\mathbf{e}_{\mathbf{k},\lambda}e^{i\mathbf{k}\cdot\mathbf{r}_p - i\omega_k t} \tag{4.52}$$

$$= -\frac{e}{m_p c}\sqrt{\frac{2\pi\hbar}{\omega_k V}}\mathbf{e}_{\mathbf{k},\lambda}e^{i\mathbf{k}\left(\mathbf{R}-\frac{m_\pi}{M_{p\pi}}\mathbf{r}\right) - i\omega_k t}. \tag{4.53}$$

We now return to equation (4.51) where we set $\mathbf{P} = 0$, which corresponds to moving to the lab frame, and the matrix element needed for Fermi's golden rule is given by

$$\mathcal{M}^{(\uparrow\downarrow)} = \frac{e}{m_p}\sqrt{\frac{2\pi\hbar}{\omega_\mathbf{k} V}}\langle(\uparrow\downarrow)p\pi^0|\frac{e^{i\mathbf{q}\cdot\mathbf{r}}}{\sqrt{V}}\frac{e^{i\mathbf{Q}\cdot\mathbf{r}}}{\sqrt{V}}|e^{i\mathbf{k}\left(\mathbf{R}-\frac{m_\pi}{M_{p\pi}}\mathbf{r}\right)}(\mathbf{e}_{\mathbf{k},\lambda}\cdot\mathbf{p})|\psi_{N\pi}\rangle\,, \tag{4.54}$$

where $\mathbf{q}$ is the wave number of the relative pion-proton system and $\mathbf{Q} = \mathbf{k}$ is the recoil. Looking at the isospin coefficient from equation (3.4), which is the factor that separates neutral pions from charged pions aside from the mass difference[5]. Inserting (3.16) and using that volume condition yields the following expression[6]

$$\mathcal{M}^{(\uparrow\downarrow)} = \frac{e}{m_p}\sqrt{\frac{2\pi\hbar}{\omega_\mathbf{k} V}}\langle(\uparrow\downarrow)p\pi^0|\frac{e^{i\mathbf{q}\cdot\mathbf{r}}}{\sqrt{V}}|e^{-i\frac{m_\pi}{M_{p\pi}}\mathbf{k}\cdot\mathbf{r}}(\mathbf{e}_{\mathbf{k},\lambda}\cdot\mathbf{p})|(\boldsymbol{\tau}\cdot\boldsymbol{\pi})(\boldsymbol{\sigma}\cdot\mathbf{r})\phi(r)\frac{p\uparrow}{\sqrt{V}}\rangle \tag{4.55}$$

Defining a new vector, $\mathbf{s} = \mathbf{q} + \frac{m_\pi}{M_{p\pi}}\mathbf{k}$ yields

$$\mathcal{M}^{(\uparrow\downarrow)} = \frac{-e}{m_\pi}\sqrt{\frac{2\pi\hbar}{\omega_\mathbf{k}}}\frac{1}{V}\left\langle(\uparrow\downarrow)\right|\langle e^{i\mathbf{s}\cdot\mathbf{r}}|(\mathbf{e}_{\mathbf{k},\lambda}\cdot\mathbf{p})(\boldsymbol{\sigma}\cdot\mathbf{r})|\phi(r)\rangle\left|\uparrow\right\rangle \tag{4.56}$$

Note the different inner products. We now consider the innermost matrix

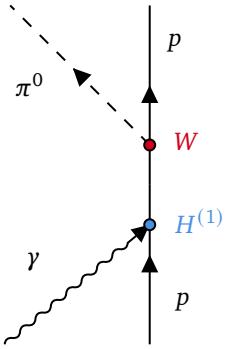

Figure 4.6: Feynman diagram of neutral pion photoproduction off protons. The blue vertex corresponds to equation (4.50) and the red vertex corresponds to equation (3.2).

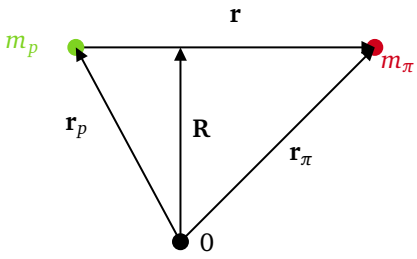

Figure 4.7: Sketch of the system. Here $\mathbf{r}_p$ is the coordinate of the proton and $\mathbf{r}_\pi$ is the coordinate of the pion. The relative coordinate is given by $\mathbf{r} = \mathbf{r}_\pi - \mathbf{r}_p$ and the coordinate of the center-of-mass is $\mathbf{R} = (m_p\mathbf{r}_p + m_\pi\mathbf{r}_\pi)/(m_p + m_\pi)$. The total mass is denoted $M_{p\pi} = m_p + m_\pi$.

5. $\langle p\pi^0|\boldsymbol{\tau}\cdot\boldsymbol{\pi}|p\rangle = 1$

6. $\int \mathrm{d}^3R\, e^{i\mathbf{k}\cdot\mathbf{R}} = V$

element in equation (4.56) where the momentum operator is inserted

$$\langle e^{i\mathbf{s}\cdot\mathbf{r}}|(\mathbf{e}_{\mathbf{k},\lambda}\frac{\partial}{\partial\mathbf{r}})(\boldsymbol{\sigma}\cdot\mathbf{r})|\phi(r)\rangle = +i(\mathbf{e}_{\mathbf{k},\lambda}\cdot\mathbf{s})\int \mathrm{d}^3r\, e^{i\mathbf{s}\cdot\mathbf{r}}(\boldsymbol{\sigma}\cdot\mathbf{r})\phi(r) \quad (4.57)$$

$$= -i(\mathbf{e}_{\mathbf{k},\lambda}\cdot\mathbf{s})\int \mathrm{d}^3r\, 3ij_1(sr)\frac{\mathbf{s}\cdot\mathbf{r}}{sr}(\boldsymbol{\sigma}\cdot\mathbf{r})\phi(r) \quad (4.58)$$

$$= (\mathbf{e}_{\mathbf{k},\lambda}\cdot\mathbf{s})(\boldsymbol{\sigma}\cdot\mathbf{r})\underbrace{\frac{4\pi}{s}\int_0^\infty \mathrm{d}r\, r^3 j_1(sr)\phi(r)}_{F(s)} \quad (4.59)$$

$$= (\mathbf{e}_{\mathbf{k},\lambda}\cdot\mathbf{s})(\boldsymbol{\sigma}\cdot\mathbf{r})F(s). \quad (4.60)$$

Where we used the spherical Bessel decomposition (C.9) in equation (4.58). In equation (4.59) we considered the angular averaging of two coordinates variables[7]. We now have an expression for the innermost matrix element in equation (4.56), which depends on the wave function $\phi(r)$. This is where the two parameters S and b enter, and ultimately these are the parameters we want to extract. It should also be noted that $F(s)$ is essentially the Hankel transform of $\phi(r)$[8]. Returning to the matrix element (4.56)

7. $\int \mathrm{d}\Omega\, n_k n_l = \frac{4\pi}{3}\delta_{kl}$, which means $\int \mathrm{d}\Omega\, r_k r_l = \frac{4\pi r^2}{3}\delta_{kl}$, where n is a unit vector.

8. See appendix C.2.

$$\mathcal{M}^{(\uparrow\downarrow)} = \frac{ie\hbar}{m_p}\sqrt{\frac{2\pi\hbar}{\omega_k}}\frac{1}{V}\langle(\uparrow\downarrow)|(\mathbf{e}_{\mathbf{k},\lambda}\cdot\mathbf{s})F(s)|\uparrow\rangle \quad (4.61)$$

$$= \frac{ie\hbar}{m_p}\sqrt{\frac{2\pi\hbar}{\omega_k}}\frac{1}{V}(\mathbf{e}_{\mathbf{k},\lambda}\cdot\mathbf{s})\langle(\uparrow\downarrow)|(\boldsymbol{\sigma}\cdot\mathbf{r})|\uparrow\rangle F(s), \quad (4.62)$$

which leads to the following expression for the norm square of equation (4.56). We do this step already to use a completeness relation for the polarisation.

$$\left|\mathcal{M}^{(\uparrow\downarrow)}\right|^2 = \frac{2\pi\hbar^3e^2}{m_p^2\omega_k V^2}\left|\mathbf{e}_{\mathbf{k},\lambda}\cdot\mathbf{s}\right|^2\left|\langle(\uparrow\downarrow)|(\boldsymbol{\sigma}\cdot\mathbf{s})|\uparrow\rangle\right|^2 F(s)^2, \quad (4.63)$$

and now evaluating

$$\sum_\lambda\left|(\mathbf{e}_{\mathbf{k},\lambda}\cdot\mathbf{s})\right|^2 = \sum_\lambda(\mathbf{e}^*_{\mathbf{k},\lambda}\cdot\mathbf{s})(\mathbf{e}_{\mathbf{k},\lambda}\cdot\mathbf{s}) \quad (4.64)$$

$$= s^2 - \frac{(\mathbf{k}\cdot\mathbf{s})^2}{k^2} \quad (4.65)$$

$$= q^2 - \frac{(\mathbf{k}\cdot\mathbf{q})^2}{k^2} \quad (4.66)$$

$$= q^2\sin^2(\theta_q), \quad (4.67)$$

where θ_q is the angle between $\mathbf{k}$ and $\mathbf{q}$, and we now have an angular dependency originating from the dot product. This step also assumes the target is unpolarised since we sum over the spin states of the proton. The subscript q is used to emphasise that this is relative to the final state momentum, also mentioned in section 2.2. The final missing term is computed by summing over the final proton spin states using (3.5)

$$\sum_{(\uparrow\downarrow)}\left|\langle(\uparrow\downarrow)|(\boldsymbol{\sigma}\cdot\mathbf{s})|\uparrow\rangle\right|^2 = s^2 \quad (4.68)$$

Using the final two expressions equation (4.67) and (4.68) with equation (4.63) and remembering the factor $1/2$ from the spin states

$$\frac{1}{2}\sum_{\lambda,(\uparrow\downarrow)}\left|\mathcal{M}_{fi}\right|^2 = \frac{\pi e^2\hbar^3}{V^2 m_p^2}\frac{1}{\omega_k}q^2\sin^2(\theta)s^2F(s)^2. \tag{4.69}$$

According to Fermi's golden rule, the transition probability is given by

$$\mathrm{d}\omega = \frac{2\pi}{\hbar}|\mathcal{M}|^2\,\rho, \tag{4.70}$$

where we can use both expressions for the density of states. We can either use the relativistic equation (2.18) or the non-relativistic equation (2.19). We will use the relativistic expression as an example but show both results at the end of the section. This leads to the final transition probability

$$\mathrm{d}\omega^0 = \frac{e^2c}{8\pi V}\frac{1}{m_p^2c^4}\frac{\mathrm{d}(\hbar cq)^2}{\mathrm{d}E_q}\frac{q^3}{k}\sin^2(\theta_q)s^2F(s)^2\mathrm{d}\Omega_q \tag{4.71}$$

which leads to the following expression for the differential cross section by considering the time it takes the photon to cross the volume, V.

$$\frac{\mathrm{d}\sigma^0(E_q,\theta_q)}{\mathrm{d}\Omega_q} = \frac{e^2}{8\pi}\frac{1}{m_p^2c^4}\frac{q^3}{k}\frac{\mathrm{d}(\hbar cq)^2}{\mathrm{d}E_q}\sin^2(\theta_q)s^2F(s)^2, \tag{4.72}$$

where the superscript is used to indicate the photoproduction of neutral pions. To get the total cross-section, we integrate all angles

$$\sigma^0 = 2\pi\int_0^\pi \mathrm{d}\theta_q\,\sin(\theta_q)\frac{\mathrm{d}\sigma^0}{\mathrm{d}\Omega_q} \tag{4.73}$$

$$= 2\pi\int_0^\pi \mathrm{d}\theta_q\,\frac{e^2}{8\pi}\frac{1}{m_p^2c^4}\frac{q^3}{k}\frac{\mathrm{d}(\hbar cq)^2}{\mathrm{d}E_q}\sin^3(\theta_q)s^2F(s)^2. \tag{4.74}$$

Equation (4.74) might seem easy to compute at first, but we have to remember $F(s)$ also contains an angular dependency originating from the magnitude of $\mathbf{s}$. Specifically, the term[9]

$$s = \sqrt{q^2 + k^2\left(\frac{m_\pi}{M_{p\pi}}\right)^2 + 2qk\frac{m_\pi}{M_{p\pi}}\cos(\theta_q)} \tag{4.75}$$

We now perform a fit of equation (4.74) to experimental data for the parameters S and b using [10, 22]. This is shown in figure 4.8 for the relativistic density of states. Data is from [23].

9. Note that equation (4.75) changes according to changes in (4.51).

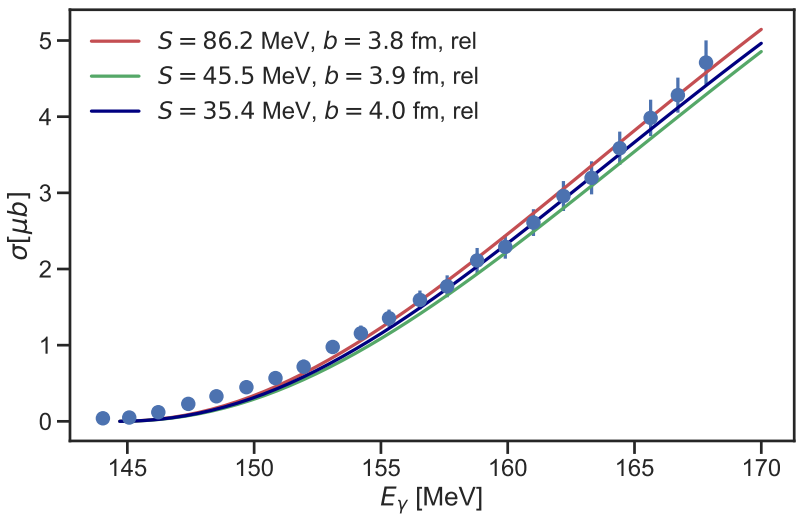

Figure 4.8: Fitted parameters to experimental data for the process $\gamma p \to \pi^0 p$ using the relativistic density of states (2.18). The fit parameters for S, b are shown inside the figure. Data is from [23]. The threshold energy for this process is 144.7 MeV.

We see that the model with explicit pions can reproduce experimental data for at least three sets of parameters. The same figure can be reproduced for the non-relativistic density of states (2.19) where the total cross section is given by

$$\sigma^0 = 2\pi \int_0^\pi \mathrm{d}\theta_q \, \frac{e^2}{4\pi} \frac{\mu_{p\pi} c^2}{m_p^2 c^4} \frac{q^3}{k} \sin^3(\theta_q) s^2 F(s)^2. \tag{4.76}$$

This is shown in figure 4.9

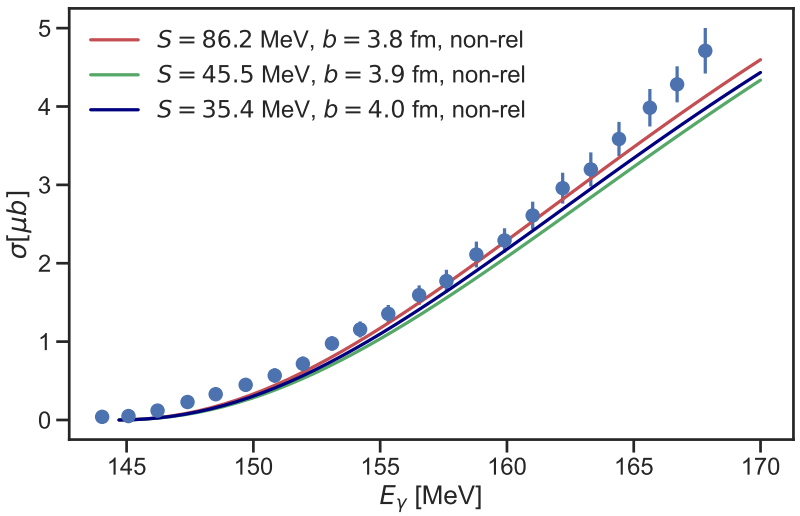

Figure 4.9: The same parameters as in figure 4.8 but using the non-relativistic density of states (2.19).

In figure 4.9, the cross-section falls off too quickly compared to figure 4.8. This indicates relativistic effects become more important as the photon energy increases. In equation (4.72), we have an expression for the angular dependency. This means that for some photon energy, we get an angular distribution. Figure 4.10 shows the differential cross section as a function of the angle θ_q compared to experimental data. Data is from [24].

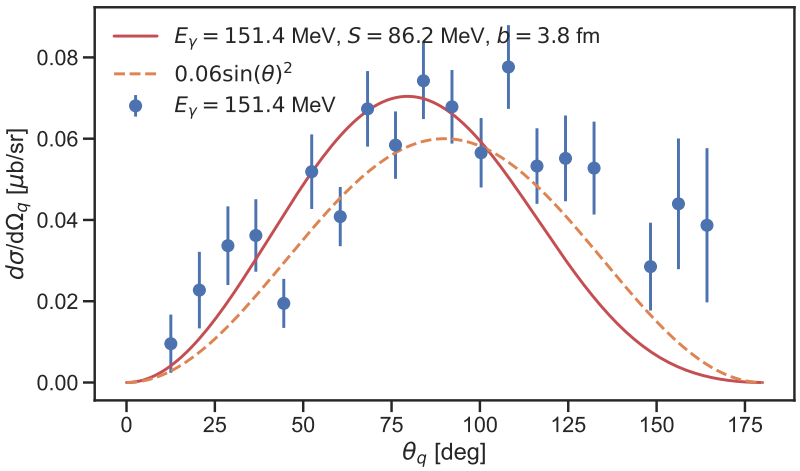

Figure 4.10: Angular distribution using equation (4.72) and experimental data from [24]. Note the dependency is not $\sin(\theta_q)^2$ since there is a contribution from $F(s)$ as well.

Figure 4.10 also shows how the angular dependency is not proportional to $\sin(\theta_q)^2$ but also has some contribution from $F(s)$. Figure 4.11 shows multiple different photon energies.

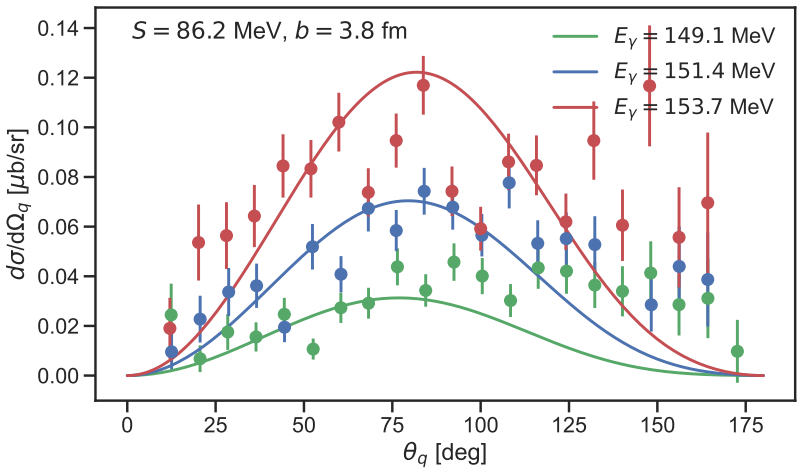

Figure 4.11: Angular distribution and experimental data for three different energies. Data is from [24]

Figures for the differential cross-section using different parameters and using the non-relativistic density of states are shown in appendix D.

The final thing we need to consider is the relative weight of the π^0 component in the wave function of the dressed proton. As in section 4.1, it is expressed as

$$C(\psi_{N\pi^0}) = \int_V \mathrm{d}^3R \int_V \mathrm{d}^3r \left|\psi_{N\pi}\right|^2 = 4\pi \int_0^\infty \mathrm{d}r\, \phi(r)^2 r^4 \tag{4.77}$$

For the three sets of parameters shown in figure 4.8, the contribution to the wave function from the π^0 is shown in figure 4.12

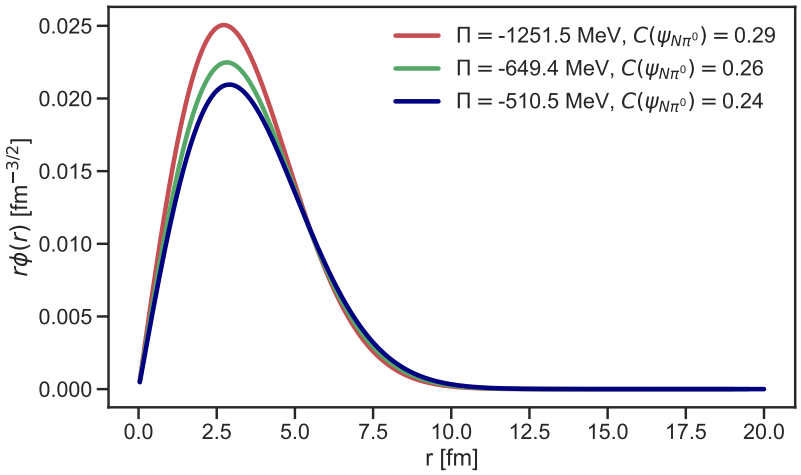

Figure 4.12: Radial wave functions using the parameters shown figure 4.8. Also includes virtual pions contribution to the dressed proton and the relative weight of the π^0 component in the wave function. The parameters S, b match the colours from figure 4.8.

From figure 4.12 we see the pion-nucleon wave function constitutes about 24% to 29% of the total wave function. This also concludes the treatment of neutral pion photoproduction off protons. This section described the general framework of how to calculate the total cross-section and contribution from the pion-nucleon system to the total wave function. These two results are shown in figure 4.8 and figure 4.12, respectively.

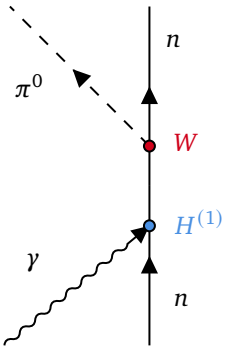

Figure 4.13: Feynman diagram of neutral pion photoproduction off protons. The blue vertex corresponds to equation (4.79) and the red vertex corresponds to equation (3.2).

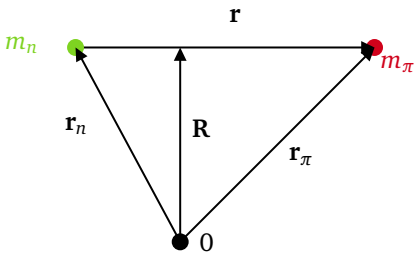

Figure 4.14: Sketch of the system. Here $\mathbf{r}_n$ is the coordinate of the proton and $\mathbf{r}_\pi$ is the coordinate of the pion. The relative coordinate is given by $\mathbf{r} = \mathbf{r}_\pi - \mathbf{r}_n$ and the coordinate of the center-of-mass is $\mathbf{R} = (m_n\mathbf{r}_n + m_\pi\mathbf{r}_\pi)/(m_n + m_\pi)$. The total mass is denoted $M_{n\pi} = m_n + m_\pi$.

4.2.2 Neutral Pion Photoproduction off Neutrons

Having considered neutral pions off protons, we now consider the closely related neutral pions off neutrons,

$$n\gamma \to \pi^0 n, \tag{4.78}$$

The Feynman diagram of the equation (4.78) is shown in figure 4.13. The key difference compared to (4.49) is that now the pion is responsible for the interaction with the electromagnetic field, and hence equation (2.7) depends on the pion, which yields the following expression

$$H^{(1)} = -\frac{e}{m_\pi c}\mathbf{A}(\mathbf{r}_\pi, t)\cdot\mathbf{p}_\pi. \tag{4.79}$$

This changes two things in comparison to equation (4.72). The mass of the proton becomes the mass of the pion, and the wave number vector becomes $\mathbf{s} = \mathbf{q} - \frac{m_n}{M_{n\pi}}\mathbf{k}$, where m_n is the mass of the neutron. Therefore the final expression for the differential cross-section using the relativistic density of states

$$\frac{\mathrm{d}\sigma^0(E_q,\theta_q)}{\mathrm{d}\Omega_q} = \frac{e^2}{8\pi}\frac{1}{m_\pi^2c^4}\frac{q^3}{k}\frac{\mathrm{d}(\hbar cq)^2}{\mathrm{d}E_q}\sin^2(\theta_q)s^2F(s)^2. \tag{4.80}$$

This leads to the following expression for the total cross-section

$$\sigma^0 = 2\pi\int_0^\pi \mathrm{d}\theta_q\,\frac{e^2}{8\pi}\frac{1}{m_\pi^2c^4}\frac{q^3}{k}\frac{\mathrm{d}(\hbar cq)^2}{\mathrm{d}E_q}\sin^2(\theta_q)s^3F(s)^2. \tag{4.81}$$

Unfortunately, no experimental data exists such that a fit can be performed. Due to the similarities between the proton and the neutron, one could expect experimental data similar to figure 4.8, which would mean different fit parameters since the pion is now responsible for the interaction with the electromagnetic field. Figure 4.15 shows the total cross-section for the process in equation (4.78) using the same fit parameters as in the previous section. The dashed lines represent the non-relativistic density of states which yields the following

$$\sigma^0 = 2\pi\int_0^\pi \mathrm{d}\theta_q\,\frac{e^2}{4\pi}\frac{\mu_{n\pi}c^2}{m_\pi^2c^4}\frac{q^3}{k}\sin^3(\theta_q)s^2F(s)^2. \tag{4.82}$$

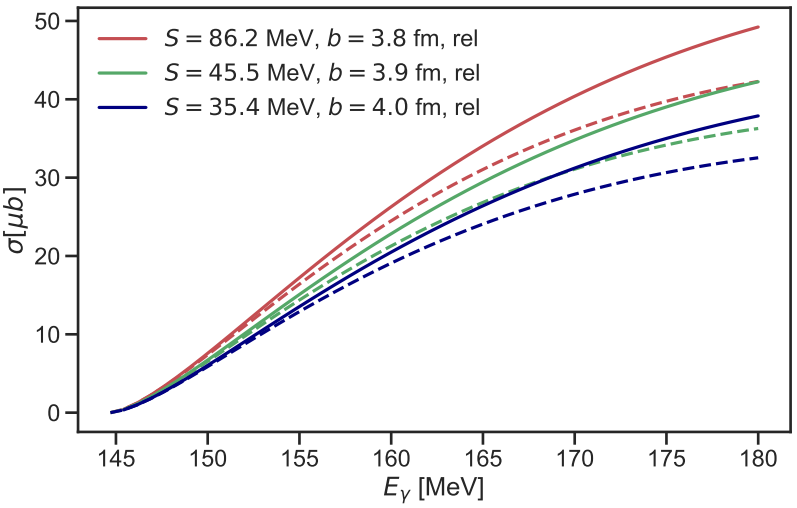

Figure 4.15: The process $\gamma n \to \pi^0 n$ with the same parameters as for neutral pion photoproduction off protons. The dashed lines represent the non-relativistic density of states (4.82). The threshold energy for this process is 144.7 MeV.

Note that the relative weight from the pion-nucleon channel will be identical to figure 4.12 since these only depend on the parameters S, b.

4.2.3 Charged Pion Photoproduction off Protons

Moving on to charged pions, we first consider the following process,

$$p\gamma \to \pi^+ n, \tag{4.83}$$

where charged pions are generated off the proton. Note that the charged pion is different in two ways compared to the neutral pion. The mass is approximately 5 MeV higher, and it contains an isospin coefficient from (3.4), which means we get the following extra contribution

$$\langle n\pi^+|\boldsymbol{\tau}\cdot\boldsymbol{\pi}|p\rangle = \sqrt{2}. \tag{4.84}$$

Carrying this factor through the derivations in section 4.2.1 amounts to a factor of 2. This means the total cross-section is given by

$$\sigma^+ = 2\pi \int_0^\pi \mathrm{d}\theta_q \, \frac{e^2}{4\pi} \frac{1}{m_p^2 c^4} \frac{q^3}{k} \frac{\mathrm{d}(\hbar c q)^2}{\mathrm{d}E_q} \sin^3(\theta_q) s^2 F(s)^2, \tag{4.85}$$

where the + indicates the production of positively charged pions. Using the non-relativistic density of states, the total cross-section can be written as

$$\sigma^+ = 2\pi \int_0^\pi \mathrm{d}\theta_q \, \frac{e^2}{2\pi} \frac{\mu_{p\pi} c^2}{m_p^2 c^4} \frac{q^3}{k} \sin^3(\theta_q) s^2 F(s)^2, \tag{4.86}$$

We once again fit equation (4.85) to experimental data from [20]. The result can be seen in figure 4.17.

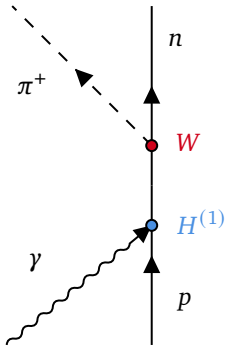

Figure 4.16: Feynman diagram of neutral pion photoproduction off protons. The blue vertex corresponds to equation (4.50) and the red vertex corresponds to equation (3.2).

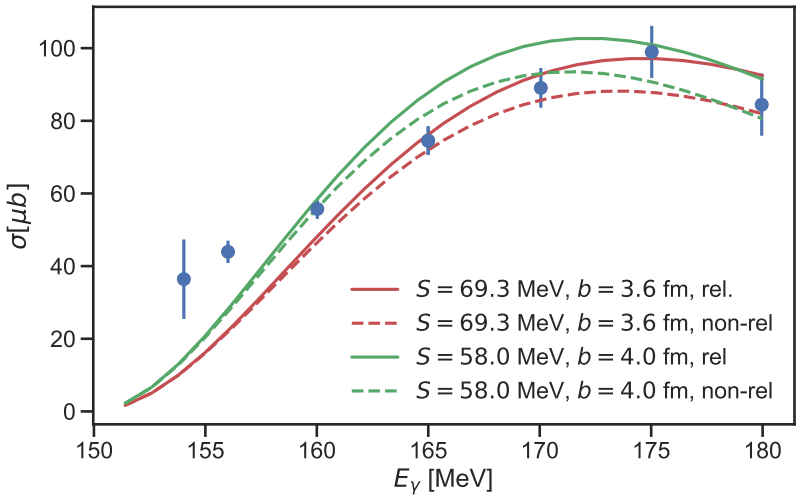

Figure 4.17: Fitted parameters for the process $p\gamma \to n\pi^+$. The parameters are shown inside the figure. The dashed lines represent the non-relativistic density of states (4.86). Data from [20]. The threshold energy for this process is 151.4 MeV.

Figure 4.17 shows the model has difficulty accurately describing the pion photoproduction of charged pions. The data points near the threshold cannot adequately be described by the parameters shown in the figure. This can be explained by the spherical Bessel function $j_1(sr)$ in the integral $F(s)$ in equation (4.85). The spherical Bessel function is 0 for $s = 0$, which means the data points near the threshold can only be included if the integral increases rapidly intermediately after the threshold. There is a trade-off since the r^3 dependency begins to dominate the integral. This means the data points near the threshold can be better described by the $j_0(qr)$ as in the dipole approximation. A combined plot is shown in figure 4.18.

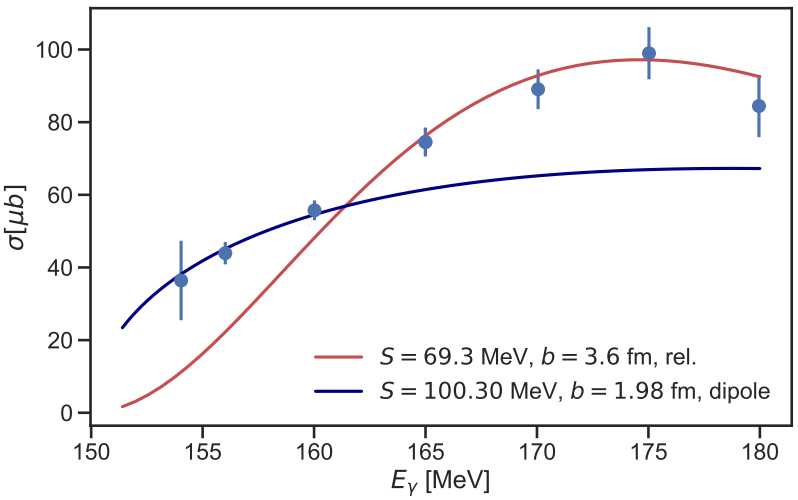

Figure 4.18: Best fit using both the dipole approximation for data points near the threshold and the exact approach for energies where the dipole approximation is no longer valid.

We now focus on the weight of the π^+ component in the wave function and the pions contribution to the mass of the dressed proton. This is shown in figure 4.19 where the colours match from figure 4.17 and figure 4.18.

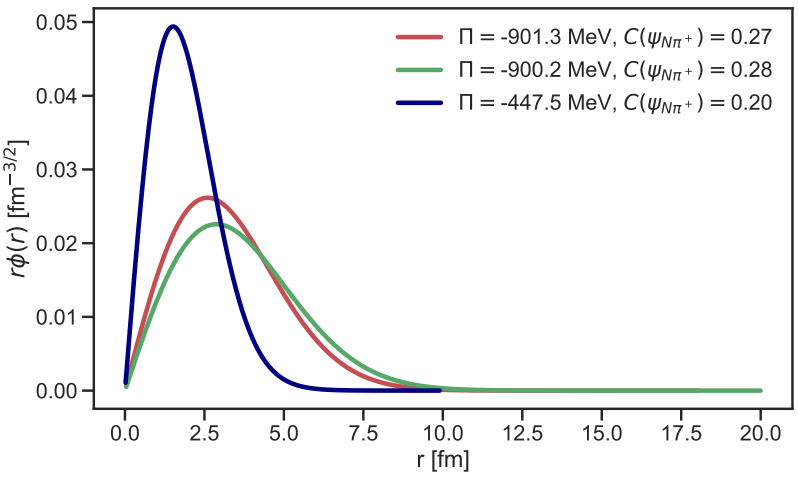

Figure 4.19: Radial wave functions using the parameters shown figure 4.17 and figure 4.18. Also includes virtual pions contribution to the dressed proton and the relative weight of the π^+ component in the wave function.

The energy is much lower when considering the parameters from the dipole approximation. The contributions are similar, which is impressive considering a difference of $S \sim 40$ MeV and $b \sim 2$ fm in the parameters.

The cross-section is one observable, which is related to how much the pion-nucleon wave function contributes to the total wave function, as shown in figure 4.19. From the formalism described in section 3 we can relate this to another observable, the charge density. We restrict the results to only consider charged pions since there is no experimental data for the process mentioned in section 4.2.3 and hence no set of parameters S, b. The two-component wave function contains the wave function $\psi_{N\pi}(\mathbf{r}_\pi, \mathbf{r}_N)$, which is a two-dimensional position wave function. This is means the probability density in a volume $d\mathbf{r}_\pi\, d\mathbf{r}_p$ at position $(\mathbf{r}_\pi, \mathbf{r}_p)$ is given by

$$\rho(\mathbf{r}_\pi, \mathbf{r}_p) = \left|\psi_{N\pi}(\mathbf{r}_\pi, \mathbf{r}_p)\right|^2, \tag{4.87}$$

and the probability of finding the pion at position $\mathbf{r}_\pi$ is then

$$\rho_\pi(\mathbf{r}_\pi) = \int d\mathbf{r}_p \left|\psi(\mathbf{r}_\pi, \mathbf{r}_p)\right|^2, \tag{4.88}$$

where we now omit the index and remind ourselves that the radial wave function is given by $\psi = r\phi$ from section 3.4. This leads to the following expression for the total charge density of the pion-nucleon system

$$\rho(\mathbf{r}) = q_\pi \int \mathrm{d}\mathbf{r}_\pi \mathrm{d}\mathbf{r}_p \left|\psi(\mathbf{r}_\pi, \mathbf{r}_p)\right|^2 + q_p \int \mathrm{d}\mathbf{r}_\pi \mathrm{d}\mathbf{r}_p \left|\psi(\mathbf{r}_\pi, \mathbf{r}_p)\right|^2, \quad (4.89)$$

where q_π and q_p are the charge of the pion and the proton, respectively. We now compute the two integrals in the center of mass using the relative coordinates illustrated in figure 4.5.

$$\rho_\pi(\mathbf{r}_{\mathrm{cm}}) = q_\pi \int \mathrm{d}\mathbf{r}_\pi \mathrm{d}\mathbf{r}_p \left|\psi(\mathbf{r}_\pi, \mathbf{r}_p)\right|^2 \delta(\mathbf{r}_\pi - \mathbf{R}, \mathbf{r}_{\mathrm{cm}}) \quad (4.90)$$

$$= q_\pi \int \mathrm{d}\mathbf{r}\, \mathrm{d}\mathbf{R} \left|\mathbf{r}\phi\left(\mathbf{R} + \frac{m_p}{M_{p\pi}}\mathbf{r}, \mathbf{R} - \frac{m_\pi}{M_{p\pi}}\right)\right|^2 \delta(\mathbf{R} + \frac{m_p}{M_{p\pi}}\mathbf{r} - \mathbf{R}, \mathbf{r}_{\mathrm{cm}}) \quad (4.91)$$

$$= q_\pi \left|\frac{M_{p\pi}}{m_p}\mathbf{r}_{\mathrm{cm}}\phi\left(\frac{M_{p\pi}}{m_p}\mathbf{r}_{\mathrm{cm}}\right)\right|^2. \quad (4.92)$$

The charge density of the nucleon can be computed in a similar manner. This means we can plot equation (4.89), which is shown in figure 4.20 as a function of the absolute radius from the center of mass.

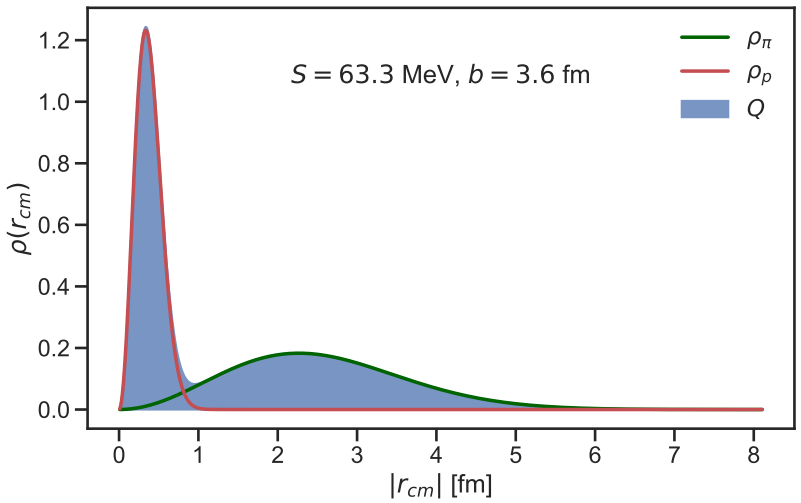

Figure 4.20: Charge density for the parameters $S = 63.3$ MeV and $b = 3.6$ fm. The charge density is normalised in such a way that the total charge Q is unity.

And similarly for the parameters using the dipole approximation

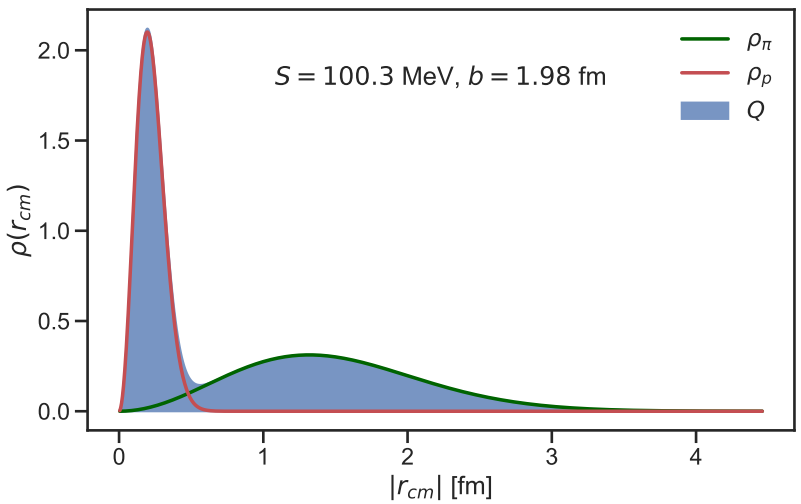

Figure 4.21: Charge density for the parameters $S = 100.30$ MeV and $b = 1.98$ fm. The charge density is normalised in such a way that the total charge Q is unity.

To complete the picture using the two-component wave function (3.1), we can imagine the bare proton as a delta function at $\mathbf{r}_{\text{cm}} = 0$ and the probability density of the proton in the pion-nucleon system moved a distance to the left on the figure 4.20. The distance corresponds to the distance away from the center of mass due to the mass difference between the proton and the pion.

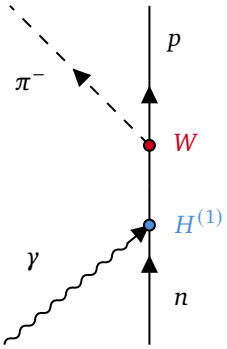

Figure 4.22: Feynman diagram of neutral pion photoproduction off protons. The blue vertex corresponds to equation (4.79) and the red vertex corresponds to equation (3.2).

4.2.4 Charged Pion Photoproduction off Neutrons

The last process to be investigated involves charged pions off a neutron,

$$n\gamma \longrightarrow \pi^- p, \tag{4.93}$$

which is also the most complicated since there is a Coulomb interaction between the two particles.

Firstly, we have to consider the dressed neutron. We can apply the same approach as we did for the dressing of the proton, but we have to include a channel where Coulomb interactions are taken into account[10]. Secondly, in the final state, we cannot use the same expansion (C.9) as we did on the plane waves. Ignoring this temporarily and we can deduce the expression for the total cross-section by combining the effects from section 4.2.2 and section 4.2.3. This means an isospin coefficient from

$$\langle p\pi^-|\boldsymbol{\tau}\cdot\boldsymbol{\pi}|n\rangle = \sqrt{2}, \tag{4.94}$$

and the mass of the pion in the denominator since the pion is responsible for the interaction with the electromagnetic field. Therefore the total cross-section is given by

$$\sigma^- = 2\pi \int_0^\pi \mathrm{d}\theta_q \, \frac{e^2}{4\pi}\frac{1}{m_\pi^2 c^4}\frac{q^3}{k}\frac{\mathrm{d}(\hbar c q)^2}{\mathrm{d}E_q}\sin^3(\theta_q)s^2F(s)^2. \tag{4.95}$$

However, the integral $F(s)$ is different since we have to account for the Coulomb interaction between the two charged particles in the final state. The behaviour of the charged particles can be described by an attractive Coulomb wave function[11], $F_1(\eta, sr)$. This leads to the final expression for the total cross-section using the regular Coulomb wave functions

$$\sigma^- = \int_0^\pi \mathrm{d}\theta_q \, \frac{e^2}{2}\frac{1}{m_\pi^2 c^4}\frac{q^3}{k}\frac{\mathrm{d}(\hbar c q)^2}{\mathrm{d}E_q}\sin^3(\theta_q)s^2\left(\frac{4\pi}{s}\int_0^\infty \mathrm{d}r\, F_1(\eta, sr)r^3\phi(r)\right)^2, \tag{4.96}$$

where η is the parameter that determines the strength of the Coulomb interaction given by

$$\eta = \frac{Z\mu_{p\pi}c\alpha}{\hbar k}. \tag{4.97}$$

Here Z is the product of the charges. Using the non-relativistic density of states, the expression for the total cross becomes

$$\sigma^- = 2\pi \int_0^\pi \mathrm{d}\theta_q \, \frac{e^2}{2\pi}\frac{\mu_{n\pi}c^2}{m_\pi^2 c^4}\frac{q^3}{k}\sin^3(\theta_q)s^2\left(\frac{4\pi}{s}\int_0^\infty \mathrm{d}r\, F_1(\eta, sr)r^3\phi(r)\right)^2, \tag{4.98}$$

The fit is performed, and the results can be seen in figure 4.23. Data is from [20].

10. This is done in appendix A.

11. This is covered in appendix C.3.

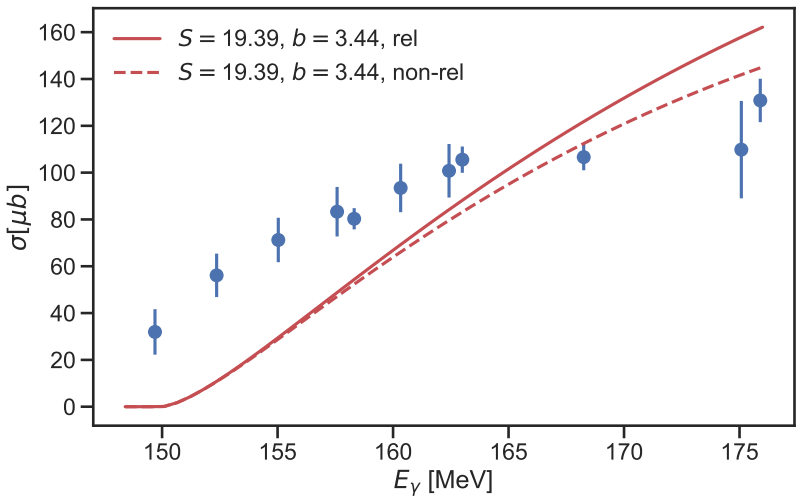

Figure 4.23: FFit of equation (4.95) to experimental data from [20].

Figure 4.23 shows a smaller range parameter b, which we would expect for two particles attracting each other. However, the model has some problems adequately describing the behaviour near the threshold. This might indicate that the one-pion approximation is insufficient, and one must include higher orders. Nonetheless, it is still possible to extract the relative weight of the $p\pi^-$ channel and the contribution to the mass of the dressed neutron. This is shown in figure 4.24

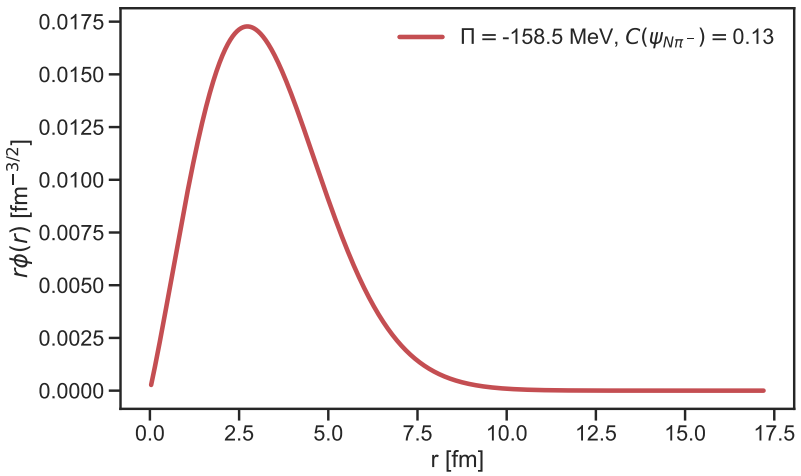

Figure 4.24: Radial wave functions using the parameters shown in the figure.

Since the strength parameter S and the range parameter b is smaller than the other processes, the contribution to the total wave function is also smaller. For the parameters shown in figure 4.23 this is 0.13%. The contribution to the mass of the dressed neutron is also much smaller, only -158.4 MeV.

Following the same approach as in section 4.2.3 we can calculate the charge density. Since we are considering a dressed neutron, the net charge must be 0. The charge density can be seen in figure 4.25

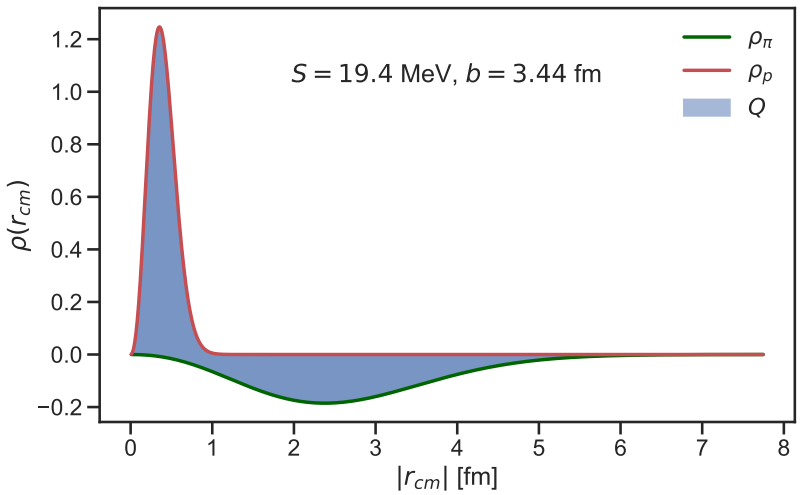

Figure 4.25: Charge density for the parameters $S = 19.4$ MeV and $b = 3.44$ fm. Note that the net charge is zero.

This concludes the treatment of pion photoproduction of pions in the model with explicit pions.

4.3 Discussion

The expression for the total cross-section for neutral pion photoproduction off protons is shown in figure 4.8 along with experimental data from [23]. The nuclear model with explicit pions can describe the behaviour of the total cross-section near the threshold when using the relativistic density of states. From figure 4.9, we see that relativistic effects become more important as the photon energy increases. By performing a fit, we can extract values for the strength parameter S and the range parameter b. We found three sets of parameters able to describe the total cross-section within the framework of the model. To further test the validity of the parameters, we compared theoretical differential cross-section to experimental data from [24]. Figure 4.11 shows a decent agreement but also that the model has some trouble describing forward scattering. In particular, the agreement is much better for angles smaller than 90 degrees which can be investigated by inspecting equation (4.72). The angular dependency originates from the sum over the polarisation index (4.64) and the magnitude of the wave number vector (4.75). Hence, the angular distribution is not a simple $\sin^2(\theta_q)$ as seen in figure 4.10. An explanation could be that the one-pion approximation is not sufficient. For instance, the two-pion contributions change the wave number vector (4.75) in such a way that the integral $F(s)$ in equation (4.72) is much higher for larger angles. Quantitatively, this claim is supported by the results in figure 4.12, where the contributions to the total wave function are shown. We see that the relative weight of the π^0 component in the wave function is within the range 24 – 29%. We expect the one-pion approximation to dominate near the threshold, but there will be a contribution from other components in the total multi-component wave function (3.1). It is difficult to estimate the contributions without explicitly solving the new physical setup. This needs new considerations about how the dressing of the nucleon is done within the two-pion framework. As more pions enter the system, new numerical challenges are revealed as the approach used in chapter 3 using coupled differential equations becomes more cumbersome as the number of particles increases. This can be circumvented by using a more general approach such as correlated Gaussians as in [2].

Figure 4.15 shows the total cross-section of the photoproduction of neutral pions off neutrons. Unfortunately, no experimental data exists near the threshold such that a fit can be performed. Once the experimental data is available, it is straightforward to use equation (4.81), and the parameters can be extracted.

Figure 4.17 shows the best fit of equation (4.85) to experimental data from [20]. The model is able to describe the experimental data if one includes the contribution from the dipole approximation as seen in figure 4.18. This leads to two sets of parameters describing the pion-nucleon system. For each set of parameters, we can estimate the charge density shown in figure 4.20 and figure 4.21. Ideally, the charge density of the pion-nucleon system would be a sum of figure 4.20 and figure 4.21 since these two contributions constitute the total cross-section, but this brings new challenges in terms of normalisation since the net charge must be unity.

Figure 4.23 showed the fit of equation (4.96) to experimental data. This is the most complicated process due to Coulomb interactions. This changes the dressing of the neutron where a three-component wave function is needed, and the final state is no longer a plane wave but a Coulomb wave. It is hard to specify what causes the fit to deviate so much from the others since Coulomb interactions are taken into account. As mentioned previously, the two-pion effects cannot be neglected even at the threshold. However, since the fit 4.23 is considerably worse than the others, it might suggest something else need to be modified. This could be the form factor mentioned in section 3.4.1 or an operator type of the form mentioned in section 3.4.3.

Chapter 5

Conclusion

In this thesis, we set out to investigate pion photoproduction in a nuclear model with explicit mesons. To do this, we first introduced the model in chapter 3 and considered how a general pion-nucleon system could be investigated. We then focused on the dressing of the proton specifically and introduced a method of solving the wave function numerically. Afterwards, we exploited the model's generality to consider different form factors and how this affected the solutions. We also considered a different operator type related to the operator found in effective field theories. This model turned out to be similar but much more numerically intensive.

In chapter 4, we began describing how pion photoproduction could be considered in a nuclear model with explicit pions. As a first approach, we used a dipole approximation which was valid only very close to the threshold. In the case of neutral pion photoproduction off protons, the model turned out to describe the total cross-section very accurately when compared to experimental data. The parameters needed for the model could also be used to describe the behaviour of the differential cross-section. In the case of neutral pion photoproduction on neutrons, experimental data is needed before the model's parameters can be extracted. A theoretical prediction was made assuming similar parameters to the case of neutral pions off protons.

In the case of charged pion photoproduction off nucleons, expressions for the total cross section and the charge density were found. The model has some problems accurately describing the behaviour of the total cross-section of charged pions, and perhaps the one-pion approximation is insufficient, and further work is needed. This would include a theoretical investigation of the two-pion approximation as well as a more suitable numerical approach.

Appendix A

Three Component Wave Function

In this appendix we cover the calculations similar to what is done in section 3.2 but for a three component wave function. In particular, we cover the dressing of the neutron and how this differs from the dressing of the proton.

A.1 Dressing of the Neutron

The dressing of the neutron differs from the dressing of the proton in the sense that Coulomb interactions are also needed in the $p\pi^-$ channel of pion photoproduction off neutrons. The three component wave function will still consists of a bare neutron and a dressed particle state but here we take the difference in particle mass and Coulomb interactions into account. Analogously to equation (3.15) and equation (3.15) we have

$$\psi_n = n \uparrow \frac{1}{\sqrt{V}}, \tag{A.1}$$

and for the pion-nucleon system where we distinguish between $N\pi^0$ and $N\pi^-$ wave functions denoted $\phi_0(r)$ and $\phi_-(r)$, respectively

$$\psi_{N\pi^0} = (\boldsymbol{\tau}\cdot\boldsymbol{\pi})(\boldsymbol{\sigma}\cdot\mathbf{r})\phi_0(r)n\uparrow\frac{1}{\sqrt{V}}, \quad \psi_{N\pi^+} = (\boldsymbol{\tau}\cdot\boldsymbol{\pi})(\boldsymbol{\sigma}\cdot\mathbf{r})\phi_+(r)n\uparrow\frac{1}{\sqrt{V}}, \tag{A.2}$$

where we omit the kets to unclutter the notation. The construction of the Hamiltonian as in equation (3.7) but here we do not want to create multipion states and apply the operator twice. We want to create a separate pion channel and hence the Hamiltonian can be written as

$$\begin{bmatrix} K_N & W^\dagger & W^\dagger \\ W & K_N + K_{\pi^0} + m_{\pi^0}c^2 & 0 \\ W & 0 & K_N + K_{\pi^-} + m_{\pi^-}c^2 + V(r) \end{bmatrix} \begin{bmatrix} \psi_n \\ \psi_{N\pi^0} \\ \psi_{N\pi^-} \end{bmatrix} = E \begin{bmatrix} \psi_n \\ \psi_{N\pi^0} \\ \psi_{N\pi^-} \end{bmatrix}, \tag{A.3}$$

where the kinetic operators are given by

$$K_N = \frac{-\hbar^2}{2m_N c^2}\frac{\partial^2}{\partial\mathbf{R}^2} \tag{A.4}$$

$$K_{\pi^0} = \frac{-\hbar^2}{2m_{\pi^0}c^2}\frac{\partial^2}{\partial\mathbf{r}^2}. \tag{A.5}$$

$$K_{\pi^-} = \frac{-\hbar^2}{2m_{\pi^-}c^2}\frac{\partial^2}{\partial\mathbf{r}^2}, \tag{A.6}$$

and W, $W^\dagger$ are the creation and annihilation of a pion, respectively. The most noticable differnce compared to equation (3.17) is the Coulomb

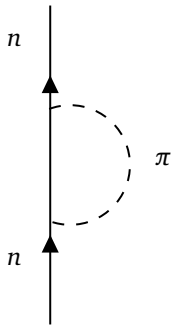

Figure A.1: Feynman diagram showing the dressing of the neutron.

interaction between charged particles. This leads to three coupled equations

$$W^\dagger \psi_{N\pi^0} + W^\dagger \psi_{N\pi^-} = E\psi_n \tag{A.7}$$
$$W\psi_n + K_{\pi^0}\psi_{N\pi^0} = (E - m_{\pi^0})\psi_{N\pi^0} \tag{A.8}$$
$$W\psi_n + K_{\pi^-}\psi_{N\pi^-} + V(r)\psi_{N\pi^0} = (E - m_{\pi^-})\psi_{N\pi^-} \tag{A.9}$$

The calculations are completely analogous to what is done in chapter 3 and the final set of equations are given by

$$\left.\begin{aligned} &12\pi \int_0^\infty \mathrm{d}r\, f(r)\phi_0(r)r^4 + 12\pi \int_0^\infty \mathrm{d}r\, f(r)\phi_-(r)r^4 = E \\ &f(r) - \frac{\hbar^2}{2\mu_{N\pi^0}}\left(\frac{\mathrm{d}^2\phi_0(r)}{\mathrm{d}r^2} + \frac{4}{r}\frac{\mathrm{d}\phi_0(r)}{\mathrm{d}r}\right) + = (E - m_{\pi^0}c^2)\phi_0(r) \\ &f(r) - \frac{\hbar^2}{2\mu_{N\pi^-}}\left(\frac{\mathrm{d}^2\phi_-(r)}{\mathrm{d}r^2} + \frac{4}{r}\frac{\mathrm{d}\phi_-(r)}{\mathrm{d}r}\right) + \frac{e^2}{r}\phi_-(r) = (E - m_{\pi^-}c^2)\phi_-(r) \end{aligned}\right\} \tag{A.10}$$

This system of equations can be solved using the method described in section 3.4. The motivation for expanding the system to a three component wave function is to include Coulomb effects for section 4.2.4. This is the solution ϕ_- in equation (A.10).

In section 3.2 we claimed that the mass difference between π^0 and $\pi^\pm$ did not affect the solutions considerably and that the two component wave function is sufficient when considering the dressing of the proton. To justify this claim consider figure A.2 a system of equations similar to (A.10) is solved without the Coulomb interaction. This means the only difference is the masses. Here the energy E corresponding to the energy solution is twice the amount in figure 3.6 since the coupled system now contains two pions.

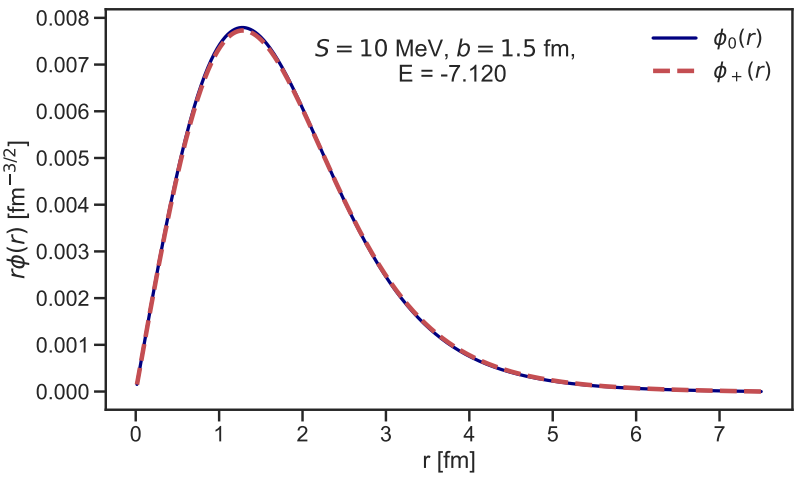

Figure A.2: Solutions to (A.10) with no Coulomb interaction. This corresponds to a three component wave function for the dressed proton. The difference in the wave function is minimal compared to the two-component wave function. The energy is equal to the sum of the two individual systems.

Appendix **B**

Nuclear Photoeffect and the Deuteron

In this appendix, we go through how to get expressions for the differential cross-section and the total cross-section from the wave function. The wave function can be obtained analytically or numerically. In this appendix, we will sketch an analytical approach to *s*-wave calculations. Considering the central potential between the proton and the neutron given by

$$U(r) = \begin{cases} -U_0, & r \leq R \\ 0 & r > R, \end{cases}$$

the radial equation is given by

$$-\frac{\hbar^2}{2m}\frac{\mathrm{d}^2u(r)}{\mathrm{d}r^2} + \left[U(r) + \frac{\hbar^2\ell(\ell+1)}{2mr^2}\right]u(r) = Eu(r). \tag{B.1}$$

This is identical to the one-dimensional Schrödinger equation with an effective potential, where the centrifugal term pushes the particle outwards. To solve this analytically, we rewrite the equation and consider the boundary conditions.

$$\frac{\mathrm{d}^2u(r)}{\mathrm{d}r^2} + \frac{M}{\hbar^2}\left[E - U(r)\right]u(r) = 0, \tag{B.2}$$

where we plugged in the expression for the reduced mass, $m = M/2$. For the deuteron, we use $E = -E_B = -2.225$ MeV [1]. This leads to the following expressions

$$\frac{\mathrm{d}^2u(r)}{\mathrm{d}r^2} + \frac{M}{\hbar^2}\left(U_0 - E_B\right)u(r) = 0, \quad r \leq R, \tag{B.3}$$

$$\frac{\mathrm{d}^2u(r)}{\mathrm{d}r^2} - \frac{M}{\hbar^2}E_B u(r) = 0, \quad r > R. \tag{B.4}$$

We introduce two variables given by

$$k = \sqrt{\frac{M}{\hbar^2}\left(U_0 - E_B\right)}, \quad \kappa = \sqrt{\frac{ME_B}{\hbar^2}}. \tag{B.5}$$

Rewriting equation (B.3) in terms of (B.5) and solving the differential equation yields

$$\frac{\mathrm{d}^2u(r)}{\mathrm{d}r^2} = -ku(r) \Rightarrow u(r) = A\sin(kr) + B\cos(kr). \tag{B.6}$$

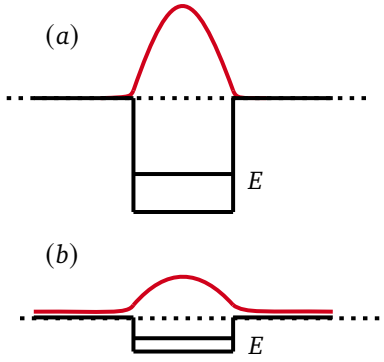

Figure B.1: Behavior of the ground state bound wave function for two potentials. (a) is an illustration of the deeper potential well case and (b) is for a shallower potential well.

Since $R(r) = u(r)/r$ and $\cos(kr)/r$ blows up as $r \to 0 \Rightarrow B = 0$ and the solution is

$$u(r) = A\sin(kr), \quad r \leq R \tag{B.7}$$

Now, considering equation (B.4)

$$\frac{\mathrm{d}^2u(r)}{\mathrm{d}r^2} = \kappa^2 u(r) \Rightarrow u(r) = Ce^{\kappa r} + De^{-\kappa r} \tag{B.8}$$

Here $Ce^{\kappa r}$ blows up as $r \to \infty$. The wavefunction must be continuous, and this means the solutions (B.6) and (B.8) must match at $r = R$. The same applies to the derivative. This leads to two equations for $r = R$.

$$A\sin(kR) = De^{-\kappa R} \tag{B.9}$$

$$Ak\cos(kR) = -D\kappa e^{-\kappa R} \tag{B.10}$$

Dividing equation (B.10) by equation (B.9) leads to

$$-\cot(kR) = \frac{\kappa}{k} \tag{B.11}$$

This equation is solved by requiring $kR = \pi/2$. Plugging in an appropriate value for $R = 1.7$ fm yields

$$\begin{aligned} U_0 &= \frac{\hbar^2\pi^2}{2mR^2} - E \\ &= \frac{\hbar^2\pi^2}{2mR^2} + E_B \\ &= 37.2\,\mathrm{MeV} \end{aligned}$$

This means the depth of the potential is 37.2 MeV.

Note that this is all for s-wave. Some considerations about the tensor force are also needed. This means we have to consider the Schrödinger equation with noncentral spin-dependent potential given by

$$\mathcal{U}(r) = \mathcal{U}_0(r) + \mathcal{U}_t(r)S_{12}, \tag{B.12}$$

where

$$\mathcal{U}_t(r) = \mathcal{U}_{tW}(r) + \mathcal{U}_{tM}(r), \tag{B.13}$$

for the space-even states we are considering with the deuteron, see table B. Considering the d-wave we introduce the angular momentum coupling $[Y_2(\mathbf{n})\chi_1]_{1M}$ of spin 1 and $\ell = 1$ to the total deuteron spin $J = 1$ and projection $J_z = M$. The same coupling but properly normalized can be written as

$$\Theta_M = \frac{1}{\sqrt{32\pi}} S_{12}\chi_{1M}. \tag{B.14}$$

To get the complete wave function of the deuteron, the expression must contain two radial parts and a spherical wave factor $1/r$

$$\Psi_M = \frac{1}{\sqrt{4\pi}}\frac{1}{r}\left(u_0(r) + \frac{1}{\sqrt{8}}u_2(r)S_{12}\right)\chi_{1M}, \tag{B.15}$$

where the two radial parts are $u_0(r)$ and $u_2(r)$ for s-wave and d-wave respectively. These must also be normalized as

$$\int_0^\infty \mathrm{d}r\,|u_0|^2 + \int_0^\infty \mathrm{d}r\,|u_2|^2 = 1. \tag{B.16}$$

Moreover, the two terms can be interpreted as a weight for the respective wave. Now using the expression for the deuteron wave function equation

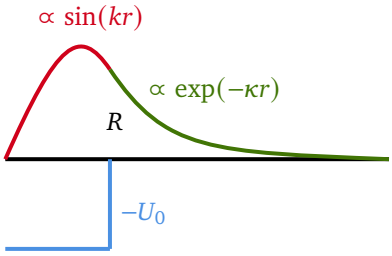

Figure B.2: The s-wave wave function for the deuteron.

	0^+	0^-	1^+	1^-
Singlet	$^1s_0$			$^1p_1$
Triplet		3_0^p	$^3s_1, ^3d_1$	$^3p_1$

Table B.1: Two nucleon states J^Π. The deuteron consists of a wave function superposition of $^3s_1 + ^3d_1$.

(B.15) we want to get an expression for the differential cross section for the nuclear photoeffect. When an absorbed photon frequency exceeds the lowest threshold of nuclear decay, the nucleus becomes excited to the continuum states. We consider the case where the decay happens through particle emission. In other words, this is the absorption of a photon that results in particle decay into the continuum. From the conservation of energy, we have

$$E_i = \hbar\omega = E_f + \epsilon, \tag{B.17}$$

where the nucleus A goes from the initial state with energy E_i to the final state with $A-1$ and energy E_f and the particle in the continuum has energy $\epsilon = \mathbf{p}^2/2m$.

The excitation of the discrete states that show resonance behaviour, and the continuum of energy states makes for a more smooth dependence. This means we can use what we know from the discrete excitation but introduce a level density ρ_f instead of the usual delta function in the expression for the differential cross section. This yields

$$\mathrm{d}\sigma_{fi} = \frac{4\pi^2\hbar}{E_\gamma c}\left|\sum_a \frac{\mathbf{e_a}}{m_a}\left\langle f\middle|(\mathbf{p}_a\cdot\mathbf{e}_{\mathbf{k}\lambda})\mathrm{e}^{i(\mathbf{k}\cdot\mathbf{r}_a)}\middle|i\right\rangle\right|^2 \rho_f, \tag{B.18}$$

where the level density is given by

$$\rho_f = \frac{Vmp}{(2\pi\hbar)^3}\mathrm{d}o. \tag{B.19}$$

Here the particle is emitted with momentum $\mathbf{p}$ into the solid angle element $\mathrm{d}o$, and E_γ is the energy of the photon. In the case of the deuteron equation (B.18) and be split into different multipolarities. The most simple is the electric dipole transition ($E1$).

In the long wavelength limit the plane wave expression reduces to unity, which means equation (B.18) for the dipole transition can be written as

$$\mathrm{d}\sigma_{E1} = \frac{\alpha mp\omega}{\hbar^2}\left|\sum_a(\mathbf{e}\cdot\mathbf{r_a})_{fi}\right|^2\frac{\mathrm{d}o}{4\pi}, \tag{B.20}$$

where the solid angle could be the direction along the motion of the proton[1].

1. Also, $V = 1$ and $\alpha = e^2/\hbar c$

When assuming an unpolarized deuteron, we can take the average over the spin states $1/3\sum_m$ and count all final polarizations $\sum_{m'}$[2]. The final state is still spin triplet since the dipole operator does not act on the spin variable. This yields

2. Note m and m'

$$\overline{\mathrm{d}\sigma_{E1}} = \frac{1}{4}\frac{\alpha mp\omega}{\hbar^2}\frac{1}{3}\sum_{mm'}\left|(\mathbf{e}\cdot\mathbf{r})_{fi}\right|^2\frac{\mathrm{d}o}{4\pi}. \tag{B.21}$$

The task is now to find an expression for the dot product in the sum. After the $E1$ transition, the final spin state remains a triplet with $S = J = 1$; the orbital and parity, however, are not the same. The final state corresponds to the p-wave, where the low-energy nuclear forces are weak, and the wavelength of the relative motion is much larger than the range of those forces. From conservation of energy, we have

$$\frac{\hbar^2k^2}{2m} = \hbar\omega - \epsilon. \tag{B.22}$$

For any direction of the relative momentum vector $\hbar\mathbf{k}$ the p-wave component must be normalized through some Legendre polynomial $P_1(\cos(\theta))$ and the spherical Bessel function $j_{\ell=1}(kr)$.[3]

3. $P_1(\cos(\theta)) = \cos(\theta)$ and $j_1(\rho) = \frac{\sin(\rho)-\rho\cos(\rho)}{\rho^2}$.

Here θ is the angle between the relative coordinate $\mathbf{r}$ and the wave vector $\mathbf{k}$ this yields

$$\psi_f(r,\theta) = 3i\cos(\theta) j_1(kr)\chi_{mm'} \tag{B.23}$$

In the s-wave transition, we get the following expression when integration over the angles of the unit vector $\mathbf{n} = \mathbf{r}/r$

$$\frac{1}{2}\left\langle f; m'\middle|(\mathbf{e}\cdot\mathbf{r})\middle|\ell = 0; m\right\rangle = -i\frac{\sqrt{\pi}}{k}(\mathbf{e}\cdot\mathbf{k})I_0\delta_{mm'}. \tag{B.24}$$

The radial integrals for the s-wave and d-wave are given by I_0 and I_2 respectively.[4] For the d-wave we have to reintroduce the tensor operator[5] S_12. Just like in the s-wave case, we have to integrate over the unit vector – this time, however, it contains four components

$$\int \mathrm{d}o\, n_i n_j n_k n_l = \frac{4\pi}{15}(\delta ij\delta_{kl} + \delta_{ik}\delta_{jl} + \delta_{il}\delta_{jk}), \tag{B.25}$$

and the d-wave contribution is given by

$$\frac{1}{2}\left\langle f; m'\middle|(\mathbf{e}\cdot\mathbf{r})\middle|\ell = 2; m\right\rangle = -i\frac{\sqrt{\pi}}{k}C_{m'm}I_2, \tag{B.26}$$

where the spin matrix element $C_{mm'}$ contains

$$C = \frac{2\sqrt{2}}{5}\left[\frac{3}{4}\left[(\mathbf{k}\cdot\mathbf{S})(\mathbf{e}\cdot\mathbf{S}) + (\mathbf{e}\cdot\mathbf{S})(\mathbf{k}\cdot\mathbf{S})\right] - (\mathbf{e}\cdot\mathbf{k})\right]. \tag{B.27}$$

Equation (B.27) can be rewritten using a trace identity[6] Skipping the calculation and moving back to equation (B.21), we have

$$\frac{1}{3}\sum_{mm'}\left|(\mathbf{e}\cdot\mathbf{r})_{fi}\right|^2 = 4\pi\left(I_0^2\cos^2(\alpha) + \frac{1}{25}I_2^2(3+\cos^2(\alpha))\right), \tag{B.28}$$

where α is the angle between $\mathbf{e}$ and the momentum of the final nucleon $\mathbf{k}$. The final steps involve averaging over the transverse polarizations of the initial photon, which also relates the angle α to the experimentally observed angle between the directions of the photon and final nucleus. This means we get the following expression

$$\overline{\cos^2(\alpha)} = \frac{1}{2}\sin^2(\theta) \tag{B.29}$$

Plugging this into equation (B.20) yields

$$\mathrm{d}\sigma_{E1} = \frac{\pi}{2}\frac{\alpha m p\omega}{\hbar^2}\left[I_0^2\sin^2(\theta) + \frac{1}{25}(6+\sin^2(\theta))I_2^2\right]\frac{\mathrm{d}o}{4\pi}, \tag{B.30}$$

and we arrive at the final expression when integrating over the angle of emitted photons

$$\sigma_{E1} = \frac{\pi}{3}\frac{\alpha m p\omega}{\hbar^2}\left(I_0^2 + \frac{2}{5}I_2^2\right). \tag{B.31}$$

It is also possible to estimate the cross-section in equation (B.31) using the initial wave function of the approximation of weak binding. Here the wave function is replaced by its exponential tail outside the range of nuclear forces. Furthermore, the contribution I_2 is neglected. This means the wave function is given by

$$\psi_i = \sqrt{\frac{\kappa}{2\pi}}\frac{\mathrm{e}^{-\kappa r}}{r}, \tag{B.32}$$

4. $I_\ell = \int_0^\infty \mathrm{d}r\, r^2 j_1(kr)u_\ell(r)$, $\ell = 0, 2$

5.

$$\begin{aligned} S_{12}(\mathbf{n}) &= 3(\boldsymbol{\sigma}_1\cdot\mathbf{n})(\boldsymbol{\sigma}_2)\cdot\mathbf{n} - (\boldsymbol{\sigma}_1\cdot\boldsymbol{\sigma}_2) \\ &= 2[3(\mathbf{S}\cdot\mathbf{n})^2 - \mathbf{S}^2] \end{aligned}$$

6.

$$\sum_{mm'}|O_{m'm}|^2 = \sum_m (O^\dagger O)_{mm} = \mathrm{Tr}\{O^\dagger O\}$$

where κ is defined in equation (B.5). Calculating the integral I_0 yields

$$\sigma = \frac{8\pi}{3}\frac{\alpha\hbar^2}{M}\frac{\sqrt{\epsilon}(\hbar\omega-\epsilon)^{3/2}}{(\hbar\omega)^3}, \tag{B.33}$$

which is rewritten in terms of the photon energy, $\xi = \hbar\omega/\epsilon$ and in terms of numerical estimates

$$\sigma(\xi) \simeq 1.2\frac{(\xi-1)^{3/2}}{\xi^3} \times 10^{-26}\,\mathrm{cm}^2. \tag{B.34}$$

The total cross-section of deuteron photodisintegration is shown in figure B.3

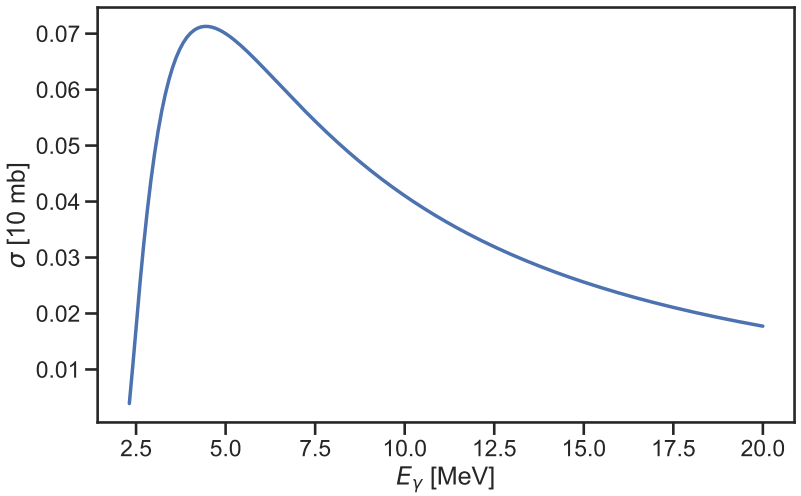

Figure B.3: Total cross section of deuteron photodisintegration as a function of photon energy divided by binding energy

Appendix C

Special Functions and Properties

This appendix covers the basics of some of the special functions that arise when discussing the properties of some operators in quantum mechanics and formulae used.

C.1 Legendre Polynomials and Spherical Bessel Functions

$$Y_\ell^m(\theta,\phi) = \frac{(-1)^{\ell l+m}}{(2\ell)!!}\left[\frac{(2\ell+1)(\ell-m)}{4\pi(\ell+m)!}\right](\sin\theta)^m \frac{\mathrm{d}^{\ell+m}}{(d\cos\theta)^{\ell+m}}[(\sin\theta)^{2\ell}]\exp\{im\phi\}, \tag{C.1}$$

which satisfy

$$Y_\ell^{*m} = (-1)^m Y_l^{-m}. \tag{C.2}$$

The spherical harmonics are connected to the Legendre polynomials

$$P_\ell(\cos\theta) = \left[\frac{4\pi}{2\ell+1}\right]^{1/2} Y_l^0(\theta). \tag{C.3}$$

Another important feature of spherical harmonics is that they form a complete set of functions over the unit sphere. Furthermore, they form an orthonormal set

$$\int \mathrm{d}\Omega\, Y_\ell^{*m} Y_{l'}^{m'} = \delta_{mm'}\delta_{ll'}. \tag{C.4}$$

Also, there exists an addition theorem for spherical harmonics

$$\sum_{m=-\ell} Y_\ell^{*m}(\theta,\phi) Y_\ell^m(\theta'.\phi') = \left(\frac{2\ell+1}{4\pi}\right)^{1/2} Y_\ell^0(\alpha). \tag{C.5}$$

The wave function of a plane wave with wave number k propagating along the z axis can be described by

$$\mathrm{e}^{ikz} = \mathrm{e}^{ikr\cos(\theta)} \tag{C.6}$$

$$= \sum_{\ell=0}^{\infty} A_\ell(r) Y_{\ell,0}(\theta), \tag{C.7}$$

where

$$A_\ell(r) = \int \mathrm{d}\Omega\, Y_{\ell,0}^*(\theta)\mathrm{e}^{ikr\cos(\theta)} = i^\ell\sqrt{4\pi(2\ell+1)}\, j_\ell(kr), \tag{C.8}$$

where the last equality shows the coefficient $A_\ell(r)$ can be expressed in terms of a spherical Bessel function $j_\ell(kr)$. Using the addition theorem

equation (C.6) yields the decomposition of a plane wave into spherical Bessel functions

$$e^{i\mathbf{k}\cdot\mathbf{r}} = 4\pi \sum_{\ell,m} i^\ell j_\ell(kr) Y_\ell^{m*}(\theta,\phi) Y_\ell^m(\theta,\phi) \tag{C.9}$$

C.2 Bessel Functions

Considering the free radial Schrödinger equation

$$\left(\frac{\mathrm{d}^2}{\mathrm{d}r^2} - \frac{\ell(\ell+1)}{r^2} + p^2\right) y(r) = 0, \quad p = \sqrt{2mE}, \tag{C.10}$$

which is an ordinary, linear, second-order differential equation and has two linearly independent solutions [25]. The solutions that are relevant in a physics context must vanish at vanish at the origin. If we consider the limit where $r \to 0$ the centrifugal term $\ell(\ell+1)$ will dominate the energy term p^2 and hence the solutions will be similar to letting $p = 0$ for which the solutions are $r^{\ell+1}$ and $r^{-\ell}$. From these two considerations we know the physically acceptable solution to equation (C.10) must be on the form $r^{\ell+1}$. These are the functions

$$\hat{j}_\ell(pr) \equiv pr\, j_\ell(pr) \equiv \left(\frac{\pi pr}{2}\right)^{1/2} J_{\ell+1/2}(pr) \tag{C.11}$$

$$= (pr)^{\ell+1} \sum_{n=0}^{\infty} \frac{(-pr/2)^n}{n!(2\ell+2n+1)!!}, \tag{C.12}$$

where the spherical Bessel functions are denoted $j_\ell(pr)$ and the ordinary Bessel functions are denoted $J_\lambda(pr)$. It is possible to express any function $f(r)$ as the weighted sum of Bessel functions. This is known as the Hankel transform given by

$$F_\lambda(k) = \int_0^\infty \mathrm{d}r\, f(r) J_\lambda(kr) r, \tag{C.13}$$

with the inverse Hankel function defined as

$$f(r) = \int_0^\infty \mathrm{d}k\, F_\lambda(k) J_\lambda(kr) k. \tag{C.14}$$

Both equation (C.13) and equation (C.14) can be expressed in terms of the spherical Bessel functions from equation (C.11) and this is essentially what is done in equation (4.59) which means the wave function $\phi(r)$ is defined through the Hankel transforms.

C.3 Coulomb Wave Functions

The Coulomb wave equation for a charged particle with arbitrary angular momentum and charge is given by

$$\nabla^2\psi + \left(k^2 - \frac{2\mu}{\hbar^2} V(r)\right)\psi = 0, \tag{C.15}$$

where μ is the reduced mass of the system. The radial wave function $u(r)$ satisfied the following differential equation

$$\frac{\mathrm{d}^2 u_\ell}{\mathrm{d}r^2} + \left(k^2 - \frac{\ell(\ell+1)}{r^2} - \frac{2\mu}{\hbar^2}\frac{Ze^2}{r}\right) u_\ell = 0, \tag{C.16}$$

where Z is the product of the charges. Two independent solutions can be found to equation (C.16) – these are called the regular and irregular Coulomb wave functions denoted $F_\ell(r)$ and $G_\ell(r)$ respectively. The regular Coulomb wave function $F_\ell(r)$ is a real function that vanishes at $r = 0$ and the behaviour of the function is described using a parameter η which describes how strongly the Coulomb interaction is

$$\eta = \frac{Zmc\alpha}{\hbar k}, \tag{C.17}$$

where m is the mass of the particle, k is the wave number and α is the fine structure constant. The solution to is given by

$$F_\ell(\eta, kr) = C_\ell(\eta)(kr)^{\ell+1}\mathrm{e}^{-ikr}\,{}_1F_1(\ell + 1 - i\eta, 2\ell + 2, 2ikr), \tag{C.18}$$

where ${}_1F_1(kr)$ is a confluent hypergeometric function and $C_\ell(\eta)$ is a normalization constant given by

$$C_\ell(\eta) = \frac{2^\ell \mathrm{e}^{-\pi\eta/2}\left|\Gamma(\ell + 1 + i\eta)\right|}{(2\ell + 1)!}, \tag{C.19}$$

where Γ is the gamma function. For numerical purposes, it is useful to use the integral representation of equation (C.18) [26, eq. 33.7.1]

$$F_\ell(\eta, \rho) = \frac{\rho^{\ell+1}2^\ell e^{i\rho-(\pi\eta/2)}}{|\Gamma(\ell + 1 + i\eta)|}\int_0^1 e^{-2i\rho t}t^{\ell+i\eta}(1 - t)^{\ell-i\eta}\,\mathrm{d}t. \tag{C.20}$$

Some examples of equation (C.20) are shown in figure C.1.

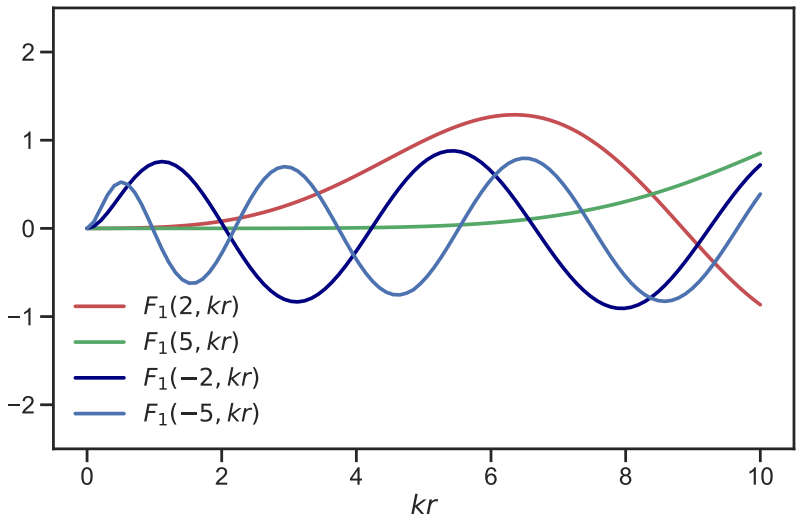

Figure C.1: Coulomb wave functions. Both in the attractive and repulsive case.

For particles without charge, we can ignore the Coulomb interaction in equation (C.16) and the solution becomes [27]

$$F_\ell(kr) = \left(\frac{\pi kr}{2}\right)^{1/2} J_{\ell+1/2}(kr) = kr\,j_\ell(kr), \quad \text{particles without charge} \tag{C.21}$$

where $J_{\ell+1/2}$ is a Bessel function and j_ℓ is a spherical Bessel function. The limit as $\eta \to 0$ is shown on figure C.2

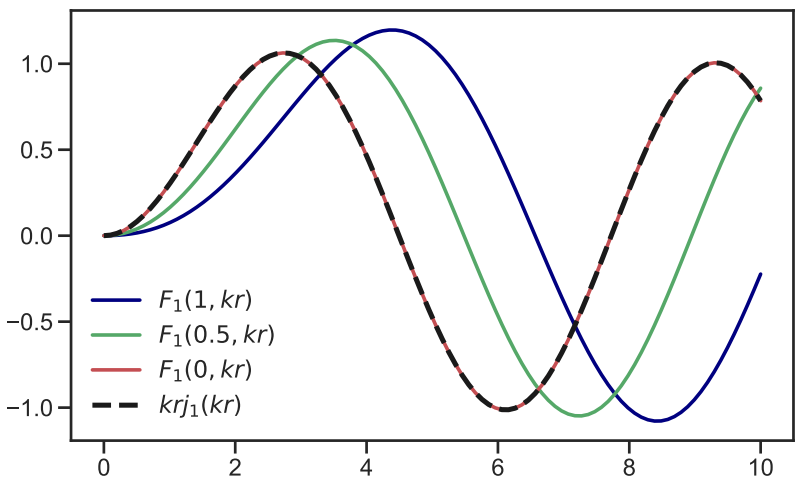

Figure C.2: Coulomb wave functions as $\eta \to 0$ which means the particles become neutral. In this case the Coulomb wave function becomes a spherical Bessel function.

Appendix D

Angular Distribution

In this appendix we see the angular distributions for other sets of parameters as mentioned in section 4.2.1.

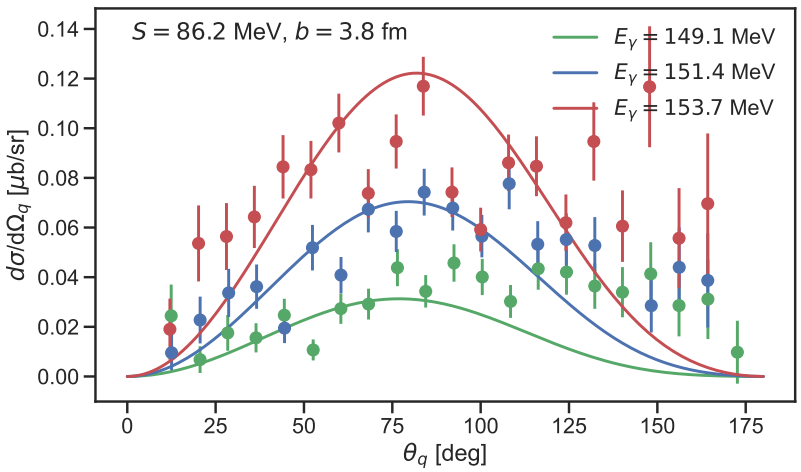

Figure D.1: Angular distribution with the parameters $S = 86.2$ MeV and $b = 3.8$ fm using the relativistic density of states

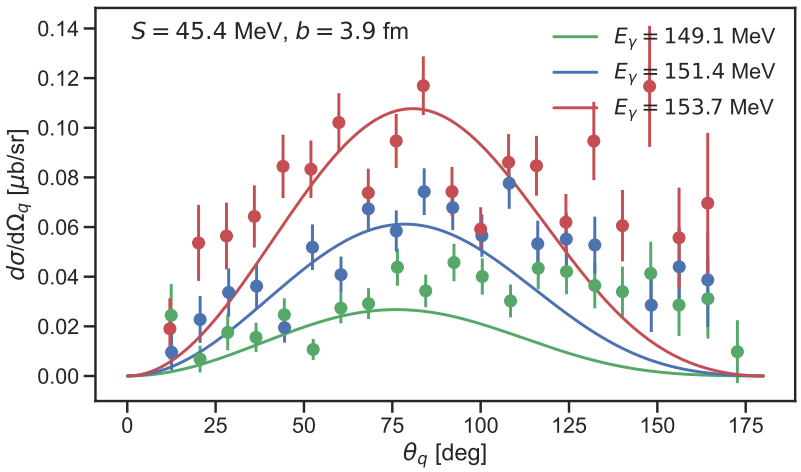

Figure D.2: Angular distribution with the parameters $S = 45.4$ MeV and $b = 3.9$ fm using the relativistic density of state

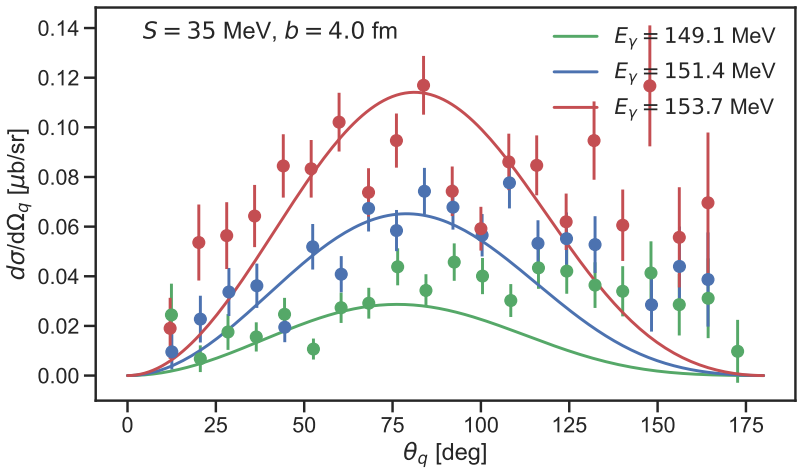

Figure D.3: Angular distribution with the parameters $S = 35$ MeV and $b = 4.0$ fm using the relativistic density of state

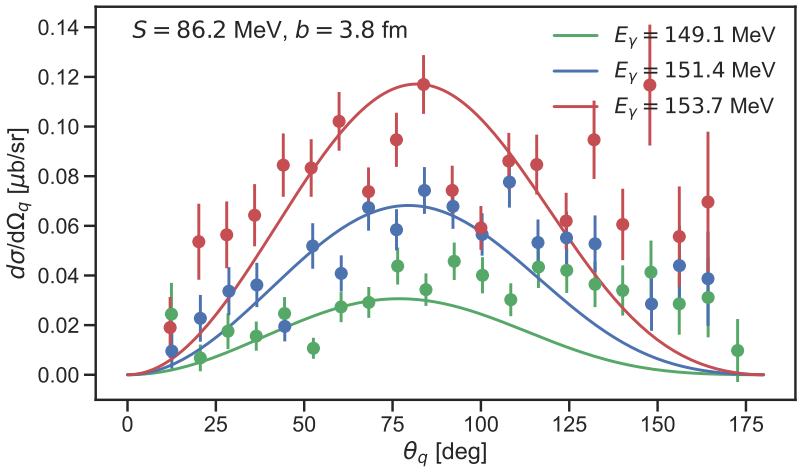

Figure D.4: Angular distribution with the parameters $S = 86.2$ MeV and $b = 3.8$ fm using the non-relativistic density of states

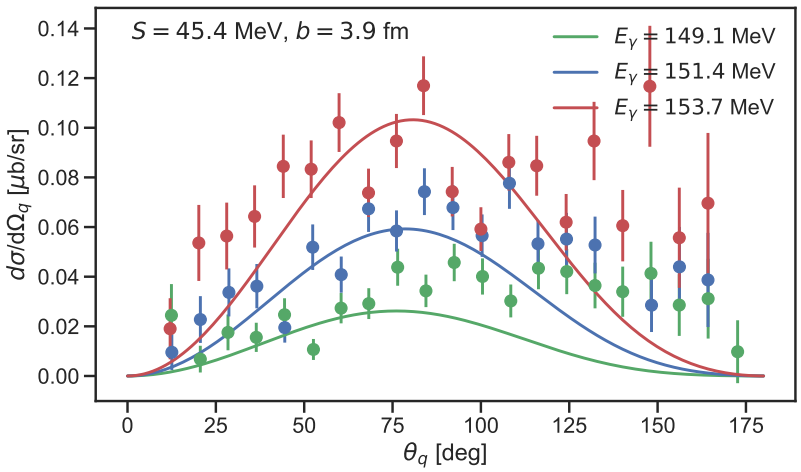

Figure D.5: Angular distribution with the parameters $S = 45.4$ MeV and $b = 3.9$ fm using the non-relativistic density of state

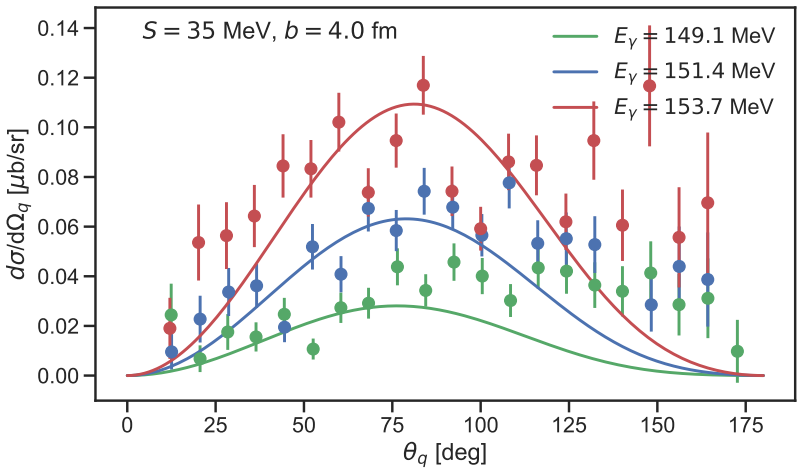

Figure D.6: Angular distribution with the parameters $S = 35$ MeV and $b = 4.0$ fm using the non-relativistic density of state

Bibliography

[1] Vladimir Zelevinsky and Alexander Volya. *Physics of Atomic Nuclei*. Wiley-VCH, first edition, 2017. ISBN 978-3-527-41350-8.

[2] D. V. Fedorov. A nuclear model with explicit mesons. *Few-Body Systems*, 61(4):40, October 2020. doi: 10.1007/s00601-020-01573-1. URL https://doi.org/10.1007/s00601-020-01573-1.

[3] Gerald A. Miller. The fundamental nature of low-energy pion-nucleon interactions, 2022. URL https://arxiv.org/abs/2208.12873.

[4] D. V. Fedorov and M. Mikkelsen. Threshold photoproduction of neutral pions off protons in nuclear model with explicit mesons. 2022. doi: 10.48550/ARXIV.2209.12071. URL https://arxiv.org/abs/2209.12071.

[5] Christopher C. Gerry and Peter L. Knight. *Introductory Quantum Optics*. Cambridge University Press, 1st edition, 2004. ISBN 978-0521527354.

[6] John David Jackson. *Classical Electrodynamics*. Wiley, 3rd edition edition, 1999. ISBN 978-0471309321.

[7] Brian R. Martin and Graham Shaw. *Nuclear and Particle Physics: An Introduction*. Wiley, 3rd edition, 2019. ISBN 978-1119344612.

[8] Philip Siemens and Aksel Jensen. *Elements of Nuclei: Many-Body Physics with the Strong Interaction*. CRC Press, 03 2018. ISBN 9780429493904. doi: 10.1201/9780429493904.

[9] Anton Vander Zee. *Group Theory in a Nutshell for Physicists*. Princeton University Press, 2016. ISBN 9780691162690.

[10] Pauli Virtanen, Ralf Gommers, Travis E. Oliphant, Matt Haberland, Tyler Reddy, David Cournapeau, Evgeni Burovski, Pearu Peterson, Warren Weckesser, Jonathan Bright, Stéfan J. van der Walt, Matthew Brett, Joshua Wilson, K. Jarrod Millman, Nikolay Mayorov, Andrew R. J. Nelson, Eric Jones, Robert Kern, Eric Larson, C J Carey, İlhan Polat, Yu Feng, Eric W. Moore, Jake VanderPlas, Denis Laxalde, Josef Perktold, Robert Cimrman, Ian Henriksen, E. A. Quintero, Charles R. Harris, Anne M. Archibald, Antônio H. Ribeiro, Fabian Pedregosa, Paul van Mulbregt, and SciPy 1.0 Contributors. SciPy 1.0: Fundamental Algorithms for Scientific Computing in Python. *Nature Methods*, 17:261–272, 2020. doi: 10.1038/s41592-019-0686-2.

[11] U.M. Ascher, R.M.M. Mattheij, and R.D. Russell. *Numerical solution of boundary value problems for ordinary differential equations*. Classics in applied mathematics. Society for Industrial and Applied Mathematics (SIAM), United States, unabridged, corr. republication. edition, 1995. ISBN 0-89871-354-4.

[12] H. W. Hammer, S. König, and U. van Kolck. Nuclear effective field theory: status and perspectives. 2019. doi: 10.48550/ARXIV.1906.12122. URL https://arxiv.org/abs/1906.12122.

[13] Steven Weinberg. Nonlinear realizations of chiral symmetry. *Phys. Rev.*, 166:1568–1577, Feb 1968. doi: 10.1103/PhysRev.166.1568. URL https://link.aps.org/doi/10.1103/PhysRev.166.1568.

[14] Steven Weinberg. *The Quantum Theory of Fields*, volume 2. Cambridge University Press, 1996. ISBN 978-0-521-55002-4. doi: 10.1017/CBO9781139644174.

[15] Anton Vander Zee. *Quantum Field Theory in a Nutshell*. Princeton University Press, 2nd edition, 2010. ISBN 9780691140346.

[16] J. C. Bergstrom, J. M. Vogt, R. Igarashi, K. J. Keeter, E. L. Hallin, G. A. Retzlaff, D. M. Skopik, and E. C. Booth. Measurement of the ^{1}H(γ, π^0) cross section near threshold. *Phys. Rev. C*, 53:R1052–R1056, Mar 1996. doi: 10.1103/PhysRevC.53.R1052. URL https://link.aps.org/doi/10.1103/PhysRevC.53.R1052.

[17] E. Mazzucato, P. Argan, G. Audit, A. Bloch, N. de Botton, N. d'Hose, J. L. Faure, M. L. Ghedira, C. Guerra, J. Martin, C. Schuhl, G. Tamas, and E. Vincent. Precise measurement of neutral-pion photoproduction on the proton near threshold. *Phys. Rev. Lett.*, 57:3144–3147, Dec 1986. doi: 10.1103/PhysRevLett.57.3144. URL https://link.aps.org/doi/10.1103/PhysRevLett.57.3144.

[18] R. Beck, F. Kalleicher, B. Schoch, J. Vogt, G. Koch, H. Ströher, V. Metag, J. C. McGeorge, J. D. Kellie, and S. J. Hall. Measurement of the p(γ,π^0) cross section at threshold. *Phys. Rev. Lett.*, 65:1841–1844, Oct 1990. doi: 10.1103/PhysRevLett.65.1841. URL https://link.aps.org/doi/10.1103/PhysRevLett.65.1841.

[19] M Fuchs, J Ahrens, G Anton, R Averbeck, R Beck, A.M Bernstein, A.R Gabler, F Härter, P.D Harty, S Hlaváč, B Krusche, I.J.D McGregor, V Metag, R Novotny, R.O Owens, J Peise, M Röbig-Landau, A Schubert, R.S Simon, H Ströher, and V Tries. Neutral pion photoproduction from the proton near threshold. *Physics Letters B*, 368 (1):20–25, 1996. ISSN 0370-2693. doi: https://doi.org/10.1016/0370-2693(95)01488-8. URL https://www.sciencedirect.com/science/article/pii/0370269395014888.

[20] W.J. Briscoe, A.E Kudryavtsev, I.I. Strakovsky, V. E V.E. Tarasov, and R.L. Workman. arthreshold π^- photoproduction on the neutron. *The European Physical Journal A*, 56(218), 2020. doi: https://doi.org/10.1140/epja/s10050-020-00221-w.

[21] Jun J. Sakurai and Jim Napolitano. *Modern Quantum Mechanics*. Cambridge University Press, 2nd edition, 2017. ISBN 978-0805382914.

[22] J J More. Levenberg–marquardt algorithm: implementation and theory. 1 1977. URL https://www.osti.gov/biblio/7256021.

[23] A. Schmidt, P. Achenbach, J. Ahrens, H. J. Arends, R. Beck, A. M. Bernstein, V. Hejny, M. Kotulla, B. Krusche, V. Kuhr, R. Leukel, I. J. D. MacGregor, J. C. McGeorge, V. Metag, V. M. Olmos de León, F. Rambo, U. Siodlaczek, H. Ströher, Th. Walcher, J. Weiß, F. Wissmann, and M. Wolf. Test of low-energy theorems for ${}^1h(\vec{\gamma},\pi^0){}^1h$ in the threshold region. *Phys. Rev. Lett.*, 87:232501, Nov 2001. doi: 10.1103/PhysRevLett.87.232501. URL https://link.aps.org/doi/10.1103/PhysRevLett.87.232501.

[24] R. Beck, F. Kalleicher, B. Schoch, J. Vogt, G. Koch, H. Ströher, V. Metag, J. C. McGeorge, J. D. Kellie, and S. J. Hall. Measurement of the p(γ,π^0) cross section at threshold. *Phys. Rev. Lett.*, 65: 1841–1844, Oct 1990. doi: 10.1103/PhysRevLett.65.1841. URL https://link.aps.org/doi/10.1103/PhysRevLett.65.1841.

[25] John R. Taylor. *Scattering Theory: The Quantum Theory of Nonrelativistic Collisions*. Dover Publications, 2nd edition, 1972. ISBN 978-0486450131.

[26] DLMF. *NIST Digital Library of Mathematical Functions*. http://dlmf.nist.gov/, Release 1.1.7 of 2022-10-15. URL http://dlmf.nist.gov/. F. W. J. Olver, A. B. Olde Daalhuis, D. W. Lozier, B. I. Schneider, R. F. Boisvert, C. W. Clark, B. R. Miller, B. V. Saunders, H. S. Cohl, and M. A. McClain, eds.

[27] Blatt and Weisskopf. *Theoretical Nuclear Physics*. Springer, New York, NY, first edition, 1958. ISBN 978-0-486-66827-7.